energies

MDPI

Review

Hydrogen Storage System Attained by HCOOH-CO_2 Couple: Recent Developments in Pd-Based Carbon-Supported Heterogeneous Catalysts

Paula Riquelme-García, Miriam Navlani-García * and Diego Cazorla-Amorós

Department of Inorganic Chemistry and Materials Institute, University of Alicante, Ap. 99, E-03080 Alicante, Spain; paula.riquelme@ua.es (P.R.-G.); cazorla@ua.es (D.C.-A.)
* Correspondence: miriam.navlani@ua.es; Tel.: +34-965-903-400 (ext. 9150)

Abstract: The present review revisits representative studies addressing the development of efficient Pd-based carbon-supported heterogeneous catalysts for two important reactions, namely, the production of hydrogen from formic acid and the hydrogenation of carbon dioxide into formic acid. The HCOOH-CO_2 system is considered a promising couple for a hydrogen storage system involving an ideal carbon-neutral cycle. Significant advancements have been achieved in the catalysts designed to catalyze the dehydrogenation of formic acid under mild reaction conditions, while much effort is still needed to catalyze the challenging CO_2 hydrogenation reaction. The design of Pd-based carbon-supported heterogeneous catalysts for these reactions encompasses both the modulation of the properties of the active phase (particle size, composition, and electronic properties) and the modification of the supports by means of the incorporation of nitrogen functional groups. These approaches are herein summarized to provide a compilation of the strategies followed in recent studies and to set the basis for a hydrogen storage system attained using the HCOOH-CO_2 couple.

Keywords: hydrogen storage; formic acid; CO_2; carbon materials; heterogeneous catalysts

Citation: Riquelme-García, P.; Navlani-García, M.; Cazorla-Amorós, D. Hydrogen Storage System Attained by HCOOH-CO_2 Couple: Recent Developments in Pd-Based Carbon-Supported Heterogeneous Catalysts. *Energies* **2024**, *17*, 260. https://doi.org/10.3390/en17010260

Academic Editor: Dmitri A. Bulushev

Received: 29 November 2023
Revised: 22 December 2023
Accepted: 29 December 2023
Published: 4 January 2024

1. Introduction

It is well known that fossil fuels have been the main energy supply since the Industrial Revolution, and their use has led to advances in both human life and industry. However, fossil fuels' depletion; massive use because of increasing energy demands, together with an increasing world population and growing prosperity; and the environmental problems associated with their use are global concerns.

Looking back over the last two centuries, we can see how the problem has been exacerbated, mainly since the middle of the 20th century. This was a period in which the terms "globalization" and "consumerism" were first coined. As a result of this, as well as uncontrolled population growth and the overexploitation of natural resources, an urgent change in global energy planning addressing the decarbonization of the energy system is now mandatory [1,2]. It is generally acknowledged that the most straightforward way to achieve a decarbonized energy system lies in the utilization of renewable energy, such as solar, wind, geothermal, or hydro energy. However, several technological, economic, and social issues arise when these renewable energies are thought to be used on a large scale at a reasonable cost [3].

The use of hydrogen is an auspicious option for the energy system. Today, hydrogen is mainly produced by steam methane reforming and coal gasification, which also generate large amounts of CO_2 (for instance, steam methane reforming emits up to 8 tons of CO_2 per ton of H_2 produced) [4]. Also, concerns related to hydrogen's storage and transportation limit its potential in the energy sector. Thus, finding alternatives for this threefold problem that limits the great potential of hydrogen (i.e., production, transportation, and storage) has been the focus of numerous recent investigations. Among the possibilities, the use of liquid

organic hydrogen carriers (LOHCs) stands out as a very interesting option that is safer and more practical and cost-effective than conventional technologies used for the storage and transport of hydrogen in the form of compressed hydrogen at either high pressure or low temperature [5–7].

Among the possible LOHCs, formic acid (FA, HCOOH) has emerged as an ideal candidate, which is not only due to its inherent properties, such as low toxicity and high stability, but also to the fact that it can be sustainably produced from biomass and biomass-derived products [8]. Another interesting pathway addressing the production of FA is from the hydrogenation of CO_2, which is particularly appealing, since it would imply an ideal carbon-neutral cycle, encompassing the following reaction [9].

$$HCOOH\ (l) \rightleftarrows H_2\ (g) + CO_2\ (g),\ \Delta G_{298K} = -32.9\ kJ{\cdot}mol^{-1} \quad (1)$$

Numerous studies have already reported that the dehydrogenation of FA (1) can be achieved under moderate reaction conditions upon the selection of a proper catalyst [10–14], while the reduction of CO_2 to FA would be more challenging.

Nevertheless, the decomposition of FA does not follow a unique pathway, but a second reaction (2) (dehydration reaction) may occur if no selective catalysts are used [15].

$$HCOOH\ (l) \rightarrow H_2O\ (l) + CO\ (g),\ \Delta G_{298K} = -20.7\ kJ{\cdot}mol^{-1} \quad (2)$$

Because of the toxicity of carbon monoxide and the reduction in hydrogen production caused by dehydration side reactions, the process needs to be optimized to shift the selectivity of FA toward the dehydrogenation step. The primary key to this lies in designing suitable catalysts. In literature, the highest conversions are obtained for homogeneous catalysis. However, such systems are less desirable from a practical application standpoint, since the reported catalysts are large metallic complexes of noble metals, such as Ru or Ir, with low stability and a high cost [16,17]. For these reasons, much effort is being devoted to designing active and selective heterogeneous catalysts. The compositions explored for the metal active phase include noble metals, such as Au [18,19], Ru [20], Pt [21,22], and Pd [23–25]. Among them, the use of Pd-based catalysts has aroused much interest due to their superior performance, but there are still some important limitations to be overcome in terms of stability and reusability [23,25]. As for the supports, carbon materials are normally preferred because of their excellent and tunable properties, as well as the versatility of these materials [26].

However, the major challenge with this storage system is not only obtaining an active and selective catalyst for dehydrogenation but also optimizing both the catalysis of formic acid dehydrogenation and the reverse reaction attaining an ideal carbon-neutral circular system, which is schematized in Figure 1 [26]. In the case of the reduction of CO_2 to FA, heterogeneous catalysts based on noble metals, such as Ru, Rh, Pt, and Pd catalysts, are also preferred [27].

Because of the relevance of the topic, this review presents the state of the art in heterogeneous catalysis for FA decomposition and carbon dioxide reduction to FA, paying particular attention to the aspects considered for the optimization of the catalysts.

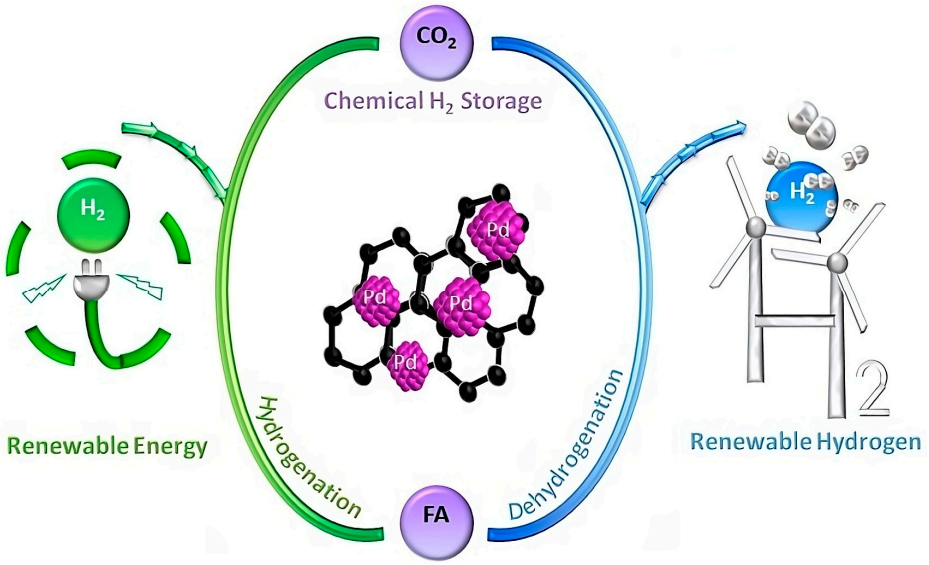

Figure 1. Chemical H_2's storage cycle using formic acid mediated by a catalyst. Green, hydrogenation CO_2 reaction; blue, formic acid dehydrogenation.

2. Dehydrogenation of Formic Acid

As mentioned in the Section 1 (Introduction), the appropriate pathway for the decomposition of FA for H_2 production is the dehydrogenation reaction (1), whereas the dehydration route (2) should be avoided because of the toxicity and poisoning effect of CO. Since the energy difference between the two decomposition pathways is very low, suitable catalysts with a high selectivity for the dehydrogenation reaction are required. Several factors influence the yield of each reaction pathway, such as temperature, substrate concentration, and the presence of additives. However, it is possible to achieve interesting catalytic performances by employing a suitable catalyst [28] and adjusting the reaction conditions [29].

Traditionally, the dehydrogenation of FA has been studied using homogeneous catalysts. In this context, studies performed by Beller [30–32] on the design of homogeneous catalysts based on transition metal complexes stand out for achieving a high catalytic activity. Despite this high catalytic activity, homogeneous catalysts are problematic in terms of their recovery and applicability, and, hence, numerous efforts have been made to develop selective heterogeneous systems for the production of H_2 from FA under mild reaction conditions.

Within heterogeneous systems, catalysts based on supported metal nanoparticles (NPs) have garnered great and growing interest. In particular, metal NPs can significantly improve the efficiency of hydrogen production because of the increase in accessible active sites [33,34]. Among all catalysts studied for this application, Pd-based ones have been hailed as highly promising alternatives. They deserve significant attention not only because of their superior CO tolerance compared to other metals but also for their ability to achieve relatively high hydrogen conversion and selectivity values at moderate temperatures [35]. Thus, numerous studies have been performed to understand and optimize Pd-based catalytic systems considering different features, such as the size of the metal NPs, metal loading, composition, electronic properties, structure, and support [36].

The Pd–support interaction has been extensively studied in these systems using porous support materials, such as silica [37–39], metal–organic frameworks [40,41], and zeolites [13]. Among the different supports, carbon materials stand out for their features, such as their resistance to basic and acidic media, their modifiable porosity, and the possibility of incorporating heteroatoms in their structure, which is of special interest in FA dehydrogenation.

As for the experimental conditions used in the dehydrogenation of FA, in the first studies in which heterogeneous catalysts were reported, a closed system was used to evaluate the catalytic performance at room temperature of very mild reaction conditions while using a very low quantity of catalysts and without incorporating additives into the reaction medium [42–44]. In such cases, the catalytic performance was assessed by analyzing the gas produced by means of gas chromatography, but information on a volumetric basis was not provided. In view of the interesting results achieved with the dehydrogenation of FA, the reaction became increasingly popular, and several research groups started to evaluate the performance of heterogeneous catalysts while scaling up the reaction using a volumetric system. Such volumetric systems are usually composed of a reactor, which contains the catalysts and the reaction mixtures (i.e., FA and additives), connected to a burette. In these studies, the results of the catalytic tests are usually expressed in the form of gas evolution profiles, considering both the CO_2 and H_2 generated during the reaction. Higher temperatures are normally used, which are limited by the boiling point of FA (i.e., 100.8 °C), and additives such as sodium formate are frequently used to enhance the performance. It should be noted that heterogeneous catalysts were also evaluated at much higher reaction temperatures when the dehydrogenation of FA was carried out in the vapor phase [45–48].

Key strategies employed in the development of high-performance carbon-supported Pd catalysts for the dehydrogenation of FA are reviewed in the following sections.

2.1. Carbon-Supported Monometallic Pd Catalysts

The study of the different properties of the active phase of Pd-based catalysts and how they affect the catalytic activity is the starting point to achieving the development of catalysts with high performance and stability.

Among the properties of catalysts, particle size is a key parameter that can be modified with the preparation method. Li et al. reported a study that investigated the catalytic activity and FA conversion of catalysts with varying sizes of Pd particles (from 2.1 to 4.5 nm) supported on carbon [49]. They prepared these catalysts with controlled particle sizes using the wet impregnation method, employing $NaBH_4$ for the reduction of the metal precursor and using sodium citrate as a stabilizing agent. The particle size variation was achieved by adjusting the reduction temperature and the sodium-citrate-to-$PdCl_2$ ratio. Their X-ray photoelectron spectroscopy (XPS) analysis revealed that as the particle size increased, the proportion of oxidized Pd (Pd^{2+} and Pd^{4+}) species decreased, while the proportion of Pd^0 increased. The catalytic activities of these Pd/C catalysts were evaluated in FA dehydrogenation in the liquid phase, and the smaller particle size catalyst (2.1 nm) exhibited the best performance with a turnover frequency (TOF) of 835 h^{-1}. The enhanced catalytic activity of smaller Pd NPs was related to their higher dispersion and a larger proportion of positively charged Pd species, leading to increased coulombic interaction with formate ions.

The composition of the surface of metal nanoparticles is commonly recognized to consist of distinct site types, including high-coordination terrace atoms and low-coordination atoms found at edges and corners. For Pd NPs, a commonly used model to comprehend the involvement of distinct sites in catalytic reactions is a cuboctahedron-shaped particle with a cubic, close-packed structure [50]. The calculated TOF values for the different sites (including low- and high-coordinated surface atoms) and the overall total number of surface atoms indicate that all surface sites are active and contribute to the FA decomposition reaction. This was the case in a study reported by Navlani-García et al., who precisely controlled the size of the Pd nanoparticles by synthesizing PVP-capped colloidal NPs using the polyol method [51]. Pd NPs between 2.7 and 5.5 nm were obtained, and the catalytic activity of the Pd/C catalysts in the dehydrogenation of FA in the liquid phase was evaluated by monitoring the H_2 production in a closed, liquid-phase system for 3 h at 30 °C. The results of the catalytic activity for the samples with different average diameters of Pd NPs are depicted in Figure 2a, showing a volcano-like relationship between the particle diameter

and H_2 production. To delve deeper into the structure–activity correlation in H_2 production with FA, calculations were conducted for catalysts of varying particle sizes, considering that the particles had a regular cuboctahedral shape with a cubic close-packed structure and adhering to the full-shell nanoparticle model. The TOF values decreased for the catalysts with sizes of NPs in the following order: 3.9 nm > 5.5 nm > 3.6 nm > 4.2 nm > 2.7 nm [51]. This observation implies that not all Pd surface sites exhibit identical catalytic activity in FA dehydrogenation. As illustrated in Figure 2b, the TOF for the low-coordinated atoms demonstrates a significant dependence on the NPs' size. In contrast, when focusing solely on the highly coordinated terrace atoms as catalytically active sites, the normalized TOF was found to be independent.

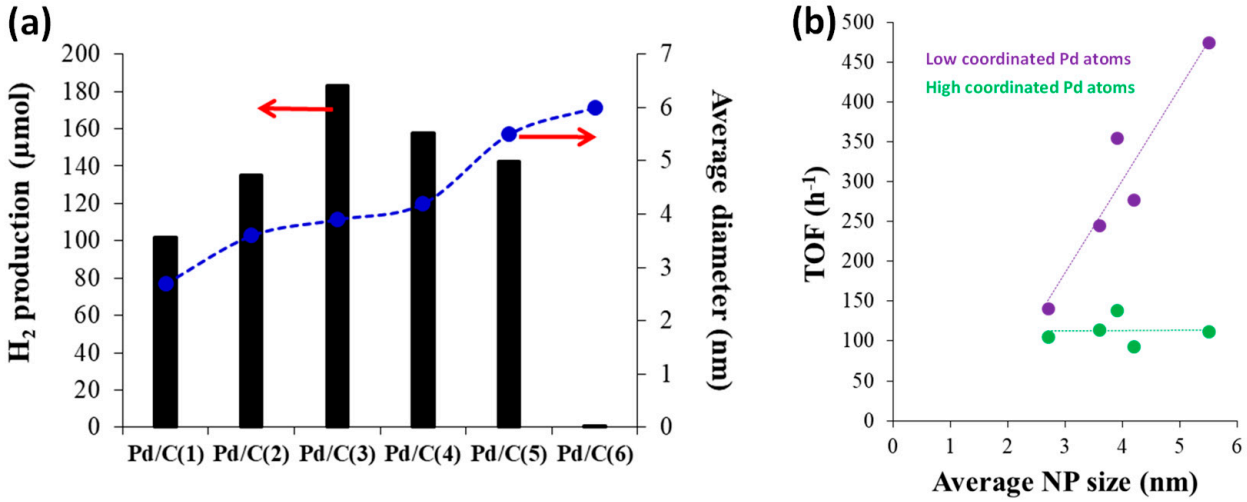

Figure 2. (**a**) Relationship between H_2 production after 3 h of reaction at 30 °C and the average NP size. (**b**) Normalized TOF values calculated on the basis of high-coordination (terrace) and low-coordination (edge and corner) as a function of the average Pd NP size. Adapted from [51].

It should be noted that the catalysts of these two studies [49,51] were synthesized following different protocols, and different experimental conditions were also used to assess the catalytic performance. So, even though smaller nanoparticles are usually preferred in catalysis, different conclusions can be drawn under certain conditions.

The incorporation of heteroatoms in carbon supports has been another widely investigated aspect of the design of catalysts used in the dehydrogenation of FA.

In particular, the incorporation of nitrogen functional groups into different types of carbon materials (carbon xerogels [52], activated carbon [53], hierarchically porous carbon [54], mesoporous carbon [55,56], etc.) and the use of different approaches to either grafting or doping the carbon material have attracted great interest over the last years [26,57,58]. The resulting N-containing materials display improved catalytic performance in the dehydrogenation of FA compared to the N-free counterpart catalysts, which is usually attributed to electronic and acid–base properties, as well as to the anchoring ability of N functional groups.

Our research group developed N-doped carbon-supported catalysts prepared from a lignocellulosic biomass residue (i.e., hemp residue) to investigate the role of nitrogen functional groups and the influence of the catalyst preparation method [53]. In that study, nitrogen incorporation was carried out with an organic reaction, and the surface nitrogen content was close to 2 at.%. The measurements of catalytic activity registered at 75 °C indicated that the developed materials displayed excellent catalytic performance, with great stability during, at least, six consecutive reaction cycles and a TOF of 8365 h^{-1}, expressed per surface Pd mol.

Yao et al. studied the effect of incorporating nitrogen groups on activated carbon (denoted as HTNC) using a high-temperature amination process [59]. The amination

process was carried out by heating the activated carbon at different temperatures (from 650 to 1050 °C) in a NH_3 flow. The XPS spectra of N 1s showed different functional groups for all of the catalysts (i.e., pyridinic N, pyrrole N, and graphitic N). The highest content of total nitrogen was observed in Pd/HTNC-950. The Pd 3d XPS spectra showed the presence of Pd^0 and Pd^{2+}, and it was seen that the content in Pd^{2+} increased with the temperature used in the amination, which confirmed the interaction between Pd and nitrogen-doped activated carbon (AC). The performance of the catalysts was tested at 30 °C in an FA/sodium formate (SF) 1:1 solution. The catalysts had remarkably different activities, and the best activity was obtained by Pd/HTNC-950, with a TOF of 1631 h^{-1}. These findings affirmed the indispensability of N species within ACs for boosting catalytic activity in FA dehydrogenation. It was claimed that the beneficial effect of N groups was due to both the electronic properties of Pd species and the high dispersion of Pd NPs achieved in the catalysts. On the one hand, it was observed that N species could modify the electron state of Pd and stabilize Pd^{2+} species, which interact with formate ions, key intermediates in FA dehydrogenation. Conversely, the HTNC effectively immobilized free Pd ions, which led to the creation of highly dispersed Pd nanoparticles. This process increased the prevalence of lower coordination sites in smaller particles, a factor that can be associated with improved performance in the reaction [60]. The stability of the catalysts was measured with five reaction cycles. Even after the fifth run, the catalytic activity of the Pd/HTNC-950 catalyst remained consistently high, underscoring the robustness of this catalyst.

Jeon et al. developed a method to dope AC with N groups that involved the pyrolysis of dicyandiamide using commercial Ketjen black [61]. The catalysts were synthesized using the wet impregnation method, with reduction assisted by $NaBH_4$. The TEM results revealed a well-dispersed arrangement of Pd nanoparticles on the N-C support, exhibiting an average size of approximately 1–2 nm. The N 1s XPS spectra of the Pd/N-C displayed the presence of C-N bonds (C=N+-C and C=N), related to the presence of N atoms in the carbon structure. The Pd 3d XPS results indicated that the electron density of the Pd species in the Pd/N-C increased because of the electrons transferred from N to Pd through the metal–support interaction. The study of the catalytic activity of these catalysts was performed at 45 °C, and Pd/N-C exhibited a better performance than Pd/C, obtaining a full conversion in 100 min. On the basis of the previously mentioned outstanding catalytic activity, a fuel cell power system was designed, linked to the FA-based hydrogen generation reactor utilizing Pd/N-C catalysts. To operate a 200 W PEMFC stack, a continuous supply of 9.5 mL min^{-1} FA was supplied to the catalytic reactor. The stack received a maximum current load of 8 A, accompanied by a lower cell voltage of around 25 V. This configuration yielded a power generation of 200 W through the utilization of fuel derived from FA dehydrogenation. To establish the durability and applicability of the integrated H_2 fuel cell stacks and the FA-based H_2 generator system employing Pd/N-C, long-term chronopotentiometric measurements were implemented. A H_2 production rate of ~3 L min^{-1} was achieved in galvanostatic conditions at a current of 6.45 A. The fuel cell demonstrated consistent performance for a duration of 80 min, with no discernible decline in stack voltage. This suggests the absence of a loss in catalytic activity for hydrogen production and indicates that there was no poisoning of the fuel cell anode catalysts, potentially caused by the formation of CO during the dehydrogenation of FA.

Chen et al. reported an efficient procedure to obtain ultrafine Pd NPs supported on N-doped activated carbon in order to study the effect of the doping method and the size of the Pd particles [62]. The preparation procedure for the nitrogen-doped activated carbon (NHPC-AC) was based on the mixing of activated carbon, $NaHCO_3$, and NH_4HCO_3 (mass ratio of 1:3.3) and then calcination at 700 °C for 1 h in N_2 flow. TEM images for the Pd/NHPC-AC catalyst indicated a good dispersion of the NPs and an average size of 1.88 nm, being smaller than the Pd/HPC-AC (2.56 nm). The XPS analysis revealed the presence of pyridinic, pyrrolic, and graphitic nitrogen. The catalytic activity was measured at 60 °C with an FA/SF molar ratio of 1/1 demonstrating better behavior for the Pd/HPC-

NAC than for the Pd/HPC-AC, reaching TOF values of 4115 h^{-1} at 60 °C and 1910 h^{-1} at 30 °C. The influence of SF was examined by varying the molar ratio of FA/SF. As the FA/SF molar ratio decreased, there was a significant enhancement of the catalytic activity, reaching a plateau when the molar ratio fell below 1:1. Furthermore, even after undergoing recycling through five cycles, the catalyst exhibited good catalytic activity, and the small average size of the NPs was preserved.

Shao et al. recently investigated a method for preparing amine-functionalized hierarchically porous carbon (TPC-NH_2) as a support for Pd NPs, which obtained excellent results in terms of catalytic activity [54]. The targeted catalyst architecture was attained by selecting MgO as a template and utilizing sodium hypophosphite to expand the pores, resulting in the formation of hierarchically porous carbon (TPC). Then, the TPC was functionalized with amino groups, and catalysts were prepared using the wet impregnation method with $NaBH_4$ reduction. With this method, ultrafine Pd NPs with an average size of 2.1 nm were obtained for the Pd/NH_2-TPC. EDS elemental mapping analysis showed a uniform distribution of the elements C, N, O, Pd and Si. The catalytic performance of Pd/NH_2-TPC at 25 °C using a 1 M FA solution without additives, revealed a high activity reaching a TOF value of 4312 h^{-1} and the increase in temperature to 60 °C achieved a TOF of 12,864 h^{-1} (see Figure 3). These results, compared with the rest of the catalysts reported for this application, using a pure FA solution without additives, show the best TOF values. The excellent catalytic activity results obtained were related to an increase in the reaction rate due to the enhancement of the mass transfer promoted by the hierarchical porous structure.

The positive effect of the presence of nitrogen functional groups has not only been observed when the reaction is performed in the liquid phase, but interesting results have also been achieved for the decomposition of FA in the gas phase. This was the case in a study by Bulushev et al., who reported that the preparation of single Pd^{2+} cations supported on N-doped carbon (Pd/N-CM) was achieved [63]. The presence of these single sites was confirmed by aberration-corrected scanning transmission electron microscopy (ac STEM). The results of the catalytic activity measured in the gas phase for Pd/N-CM at 100 °C showed a TOF value of 0.121 s^{-1}. Following ex situ reduction in hydrogen at 300 °C, the outcomes of the X-ray photoelectron spectroscopy (XPS) and near-edge X-ray absorption fine structure (NEXAFS) investigations revealed the presence of Pd species in a Pd^{2+} state, coordinated by nitrogen species within the support. Furthermore, extended density functional theory (DFT) calculations confirmed the crucial involvement of an isolated Pd atom as the active site in FA decomposition, leading to the generation of an adsorbed hydrogen atom and a carboxyl fragment. However, this activity was only viable when the Pd atoms were coordinated by a pair of pyridinic-type nitrogen atoms located at the open edge of the graphene sheet. Thus, the nitrogen doping of the carbon support plays a pivotal role in creating and stabilizing these new active Pd sites. Bulushev also reported the synthesis of catalysts based on Pd active sites on covalent triazine frameworks to investigate the effect of the support and the interaction with the Pd sites [64]. The Pd catalysts were prepared by the impregnation with the supports: 5,6,11,12,17,18-hexaazatrinaphthylene-2,8,14-tricarbonitrile (hatnCTF); 4,4′-malonyldibenzonitrile (acacCTF); and g-C_3N_4. By means of HRTEM and HAADF/STEM, the formation of the nanoparticles was observed in Pd/acacCTF and Pd/g-C_3N_4, which had average sizes of 5.2 and 3.0 nm, respectively, while for the Pd/hatnCTF only single atoms were observed and for Pd/acCTF the presence of these could also be appreciated. Nevertheless, Pd/g-C_3N_4 only presented Pd in the form of NPs. The Pd/hatnCTF sample presented a higher proportion of Pd^{2+} sites than the rest of the samples. It was shown that the single atoms in Pd/hatnCTF were found as Pd^{2+}-C_1N_3 sites, and the Pd/acacCTF sample contained single-atom Pd^{2+}-O_4 sites. The presence of a significant proportion of metal NPs in Pd/acacCTF was also confirmed. The catalytic activity measured in the gas phase showed the best performance for Pd/hatnCTF, with a TOF of 0.28 s^{-1} at 180 °C. Additionally, a stability assessment was conducted for Pd/hatnCTF that showed no deactivation at 180 °C, and there was even a slight increase

in FA conversion within the initial 5 h of the test. These results could be attributed to the presence of single-atom Pd sites (Pd-C_1N_3) in the Pd/hatnCTF, while in the Pd/acCTF, the Pd single-atom Pd-O_4 sites were not active for the reaction; thus, the low activity observed for this catalyst is only due to the presence of NPs.

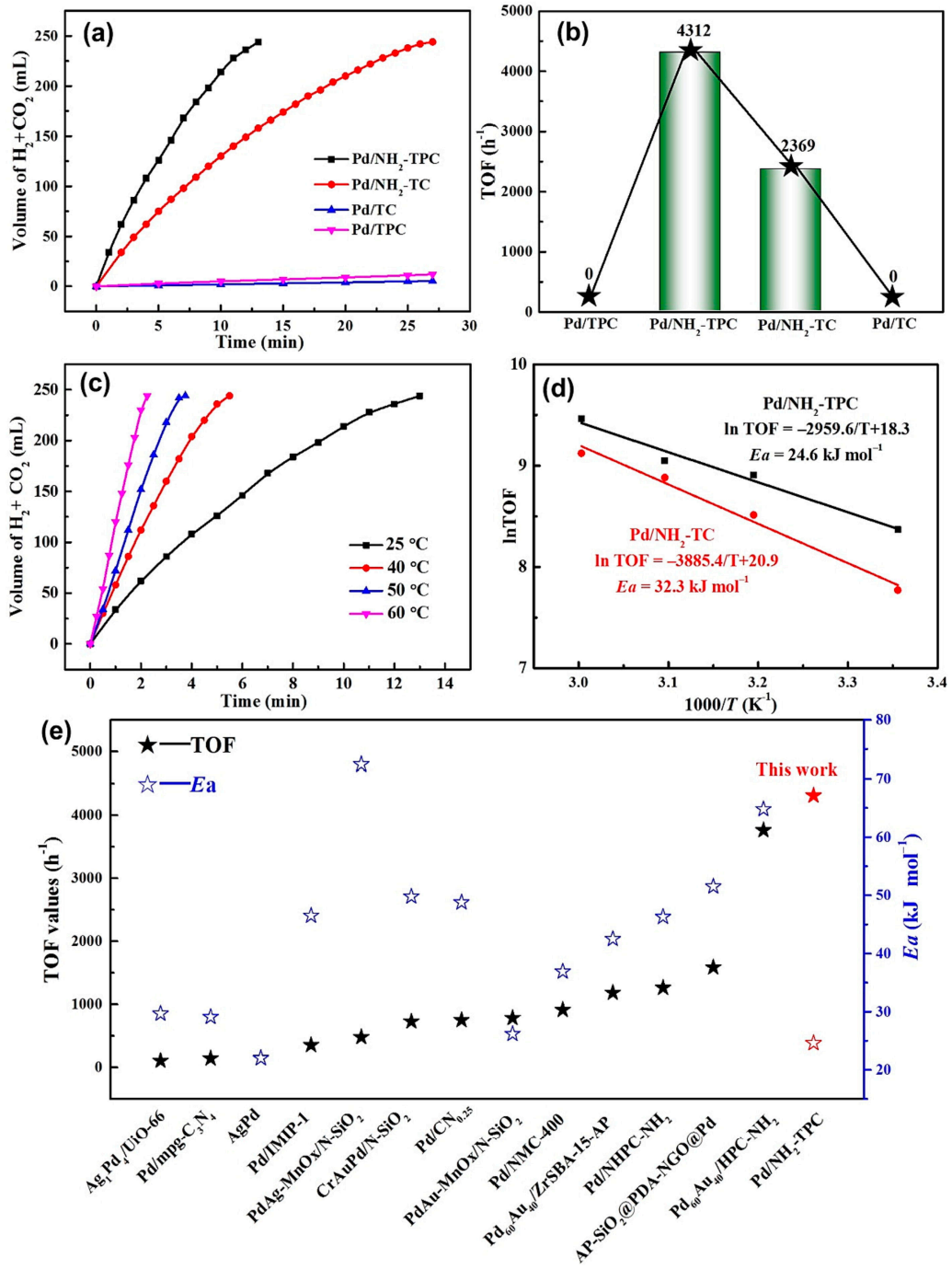

Figure 3. (**a**) Time-dependent gas production for various Pd-based catalysts during the decomposition of FA and (**b**) related TOF values; (**c**) plot of gas generation from FA as a function of time at different temperatures; (**d**) Arrhenius plot of FA dehydrogenation (rection conditions: 5 mL and 1.0 M FA; nPd/nFA = 0.0037); (**e**) comparison of the catalysts for the additive-free FA dehydrogenation described in the literature. Reprinted with permission from Ref. [54]. 2022, Elsevier.

2.2. Carbon-Supported Multimetallic Pd-Based Catalysts

Exceptional outcomes have been attained with Pd-based bimetallic catalysts designed as alloys or core–shell structures. In these configurations, the electronic promotion of Pd species occurs through the charge transfer from the other component. The favorable effects of the construction of multimetallic catalysts extend to mitigating deactivation caused by poisonous intermediates such as CO. Moreover, these catalysts attenuate hydrogen adsorption on the NPs' surface, facilitating the combination of two hydrogen atoms to form an H_2 molecule [65,66].

Specifically, extensive research has been conducted on systems incorporating Pd in conjunction with other noble metals. Pd-Ag-based catalysts, in particular, exhibit remarkable performance. This can be attributed to the electron-rich Pd species resulting from electron transfer from Ag to Pd due to the difference in electronegativity (2.2 and 1.9, according to the Pauling scale, for Pd and Ag, respectively) [67].

Navlani-García et al. studied colloidal bimetallic PdAg NPs that were prepared using the polyol method and supported in a commercial activated carbon to understand the effect of alloying Pd with Ag and to elucidate the optimal composition under the experimental conditions used in the study [44]. The study was performed with different Pd/Ag ratios, as well as different PVP/metal ratios. TEM micrographs showed how the addition of Ag in small proportions (Pd1Ag0.5, Pd1Ag1, and Pd1Ag2) reduced the particle size compared to the monometallic catalysts. The catalytic efficiency of the PdAg/C catalysts in the FA dehydrogenation reaction was assessed by observing the hydrogen produced over a period of 3 h at 30 °C. The high influence of the Pd/Ag ratio, as well as the PVP/metal ratio, could be appreciated, with the catalyst with the best activity being Pd1Ag2, with PVP/M = 1. The EXAFS measurements for the Pd1Ag2/C confirmed the heteroatomic Pd-Ag bonding in the studied catalysts. The analysis of the XPS spectra indicated that Pd and Ag were predominantly present in metallic form, but a minor presence of the oxidized forms (Pd^{2+} and Ag^{+}) was observed for both elements. The presence of oxidized species was attributed to the electron-withdrawing nature of PVP facilitated by the C=O groups, leading to metal surfaces with a deficit of electrons.

Recently, Kim et al. investigated different Pd:Ag compositions for elucidating the alloying effect on PdAg NPs supported on carbon nanotube (CNT) catalysts [68]. The catalysts were prepared with the deposition–precipitation method using CNTs as the support. The total content of Pd and Ag was fixed at 5 wt.% while varying their molar ratios. The Pd-binding energy, obtained using XPS, showed the highest shift to lower energy for the catalyst with an Ag/Pd ratio of 3/7, which can be attributed to increased interactions among the metals. The initial TOF values showed a volcano-type curve according to the Ag/Pd ratio, the Pd_7Ag_3/CNT catalyst presented the highest value. In this sense, kinetic isotopic effect (KIE) experiments were performed to investigate the alloy effect. The KIE results showed lower values with an increasing Ag content, reaching a minimum at which it remained constant for Pd/Ag molar ratios of 7:3. This lower KIE (k_h/k_d) value can be associated with a weaker C-H bond, which facilitates the breaking of this bond of the adsorbed $HCOO^-$, thereby easing the course of the overall reaction. In that investigation, the alloying impact of Ag on Pd was elucidated as an electronic modification of Pd, causing the molecular orbital of the adsorbed $HCOO^-$ to exhibit a weaker C–H bond. Consequently, this facilitated the cleavage of the C–H bond in $HCOO^-$*, leading to increased activity in the dehydrogenation of FA over the PdAg/CNT catalysts.

The positive effect of the incorporation of nitrogen functional groups has also been evidenced for bimetallic PdAg catalysts. For instance, Nabid et al. reported the effect of the formation of Ag-core Pd-shell NPs supported on nitrogen-doped graphene carbon nanotube aerogel (Ag@Pd/N-GCNT) [69]. In that study, a nitrogen-doped hybrid aerogel incorporating graphene and CNTs was developed. Subsequently, the aerogel was loaded sequentially with Ag and Pd to attain core–shell NPs. The results indicated that, in addition to the N sites, the graphene CNT aerogel offered supplementary stabilization points for the NPs, preventing their aggregation. Among the tested compositions, catalysts with an

Ag/Pd molar ratio of 1/1 exhibited the highest activity, achieving a TOF value of 413 h^{-1} at 25 °C.

In our research group, catalysts based on Pd and PdAg NPs were designed from activated carbons prepared from a biomass residue (almond shell) and doped with nitrogen groups to elucidate the effect of the catalysts' preparation [70]. Two sets of catalysts were prepared, one using the wet impregnation method with reduction by $NaBH_4$ and the other with the reduction step by $NaBH_4$ omitted whereby the metals were expected to be reduced in situ during the reaction. The results of the catalytic activity measured at 75 °C showed significant differences between the prereduced catalysts and those that were not. The reduced PdAg catalysts showed better activity than the monometallic counterparts. In the nonprereduced bimetallic catalysts, an induction period was observed at the beginning of the gas–time curve. The PdAg/N-AS showed the best performance, achieving an initial TOF of 1577 h^{-1}, and the good stability of the catalyst was demonstrated after six consecutive reaction cycles.

Furthermore, for Pd bimetallic catalysts, other noble metals such as Au have been used to form PdAu alloys for the dehydrogenation of FA. Jiang et al. reported a study in which AuPd NPs supported on N-doped carbon nanosheets (n-CNS) were assessed with the objective of demonstrating the role of the Au and N groups in the reaction performance [71]. The synthesis procedure is described in Figure 4, and it consists, first, of a hydrothermal treatment of a solution of graphitic carbon nitride (g-C_3N_4) and glucose followed by calcination, using different temperatures. The AuPd catalysts were prepared using wet impregnation with a reduction step. The images obtained by HAADF-STEM and STEM-EDX confirmed the homogeneous distribution of N, and it was also seen that the Au and Pd signals were located at the same position, which firmly indicated the existence of AuPd alloy. The highest activity was obtained for AuPd/n-CNS-Th-160 (hydrothermal treatment at 160 °C), which achieved a TOF of 459 h^{-1} at 25 °C and a value of 1896 h^{-1} at 60 °C with 100% selectivity to CO_2 and H_2. Furthermore, the study demonstrated that the catalytic activity did not exhibit a direct correlation with the mass of nitrogen dopant. Conversely, a pivotal role was attributed to the nitrogen-bonding configurations, with a demonstrated improvement in the interactions between the AuPd metal NPs and support when a higher ratio of graphitic N to pyridinic N was present.

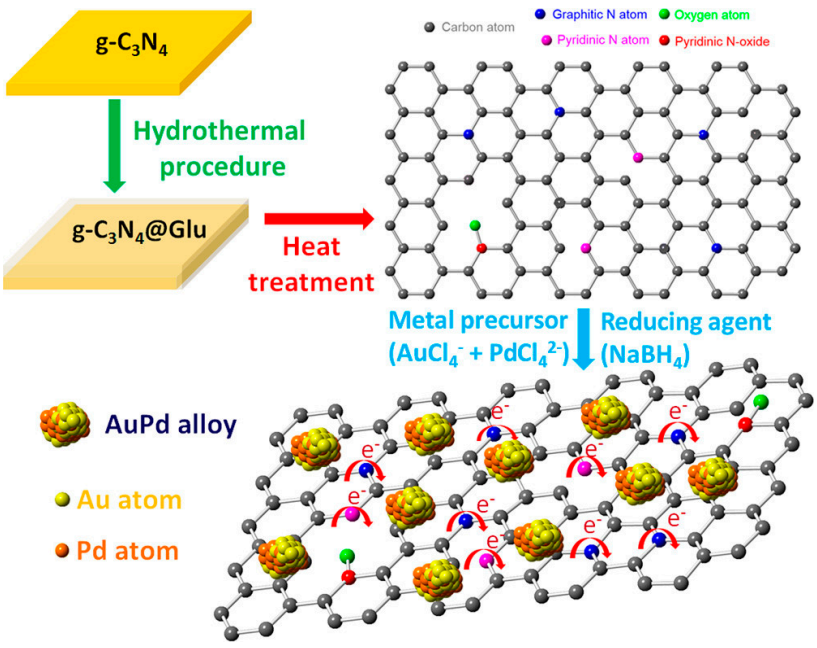

Figure 4. Schematic illustration of the preparation procedure for AuPd/n-CNS nanocatalyst. Reprinted with permission from Ref. [71].

Hong et al. developed a simple method for the immobilization of PdAu NPs on commercial carbons to highlight the importance of the metal–support interaction [72]. The method consisted of the wet mixing of the metal precursors, using L-arginine (LA) as a mediating reagent, with MSC-30 and Vulcan XC-72R and a reduction step. The catalyst formed by PdAu NPs supported on MSC-30 was denoted as Pd_1Au_1/30-LA, and the one supported on Vulcan XC-72R was denoted as Pd_1Au_1/72-LA. Severe differences in the catalysts were observed. Firstly, the mean particle size, obtained with TEM, was smaller for Pd_1Au_1/72-LA, suggesting the importance of the metal–support interaction. Pd_1Au_1/30-LA showed exceptional performance in the dehydrogenation of FA using a pure FA solution at 60 °C reaching a TOF value of 8355 h^{-1}. Moreover, the stability of that catalyst was studied for five consecutive reaction cycles, which revealed its excellent durability. However, when the reaction was studied using a 1:3 molar FA/SF solution, the catalyst with the best activity was Pd_1Au_1/72-LA, obtaining a TOF of 11,958 h^{-1} at 60 °C, and the stability test also proved its high durability. In addition, LA was found to play an important role in modulating the size and dispersion of the NPs.

Noble metal-based architectures are usually preferred for their reported catalytic properties. Nevertheless, the limited availability and elevated costs of these metals have spurred the exploration of alternative non-noble metals, including transition metals, such as Co, Ni, and Cu.

Navlani-García et al. studied PdCo-based bimetallic systems with different Pd/Co ratios supported on *g*-C_3N_4 to understand the effect of enhanced catalytic activity after Co addition on these catalysts [73]. The Pd-based catalysts were synthesized using an impregnation method, mixing *g*-C_3N_4 with the appropriate amount of Na_2PdCl_4 and $Co(NO_3)_2$. The catalytic activity evaluated at 75 °C for the different compositions of NPs showed that the gradual addition of Co resulted in outperforming catalysts until the optimal composition was reached in the sample PdCo/*g*-C_3N_4 (1/0.7), achieving a TOF value of 1193 h^{-1}. The additional introduction of Co was proved to be ineffective and counterproductive in terms of FA dehydrogenation capability, that could be attributed to the partial shielding of the active sites in the Pd NPs by the excess of cobalt. The XPS spectra of Pd 3d revealed a slight shift toward lower binding energies in the PdCo catalysts compared to monometallic Pd. This shift verified the presence of alloyed NPs and implied the generation of electron-rich Pd species on the PdCo particles. This phenomenon could be ascribed to the transfer of electrons from Co to Pd, as suggested by their respective electronegativities. The beneficial influence of the alloy system on the catalysis of FA dehydrogenation was corroborated by potential energy profiles generated using DFT calculations. Pd_{43} and $Pd_{22}Co_{21}$ clusters were employed as models for monometallic and alloy NPs, respectively. Considering the suggested reaction mechanism (Figure 5), the $Pd_{22}Co_{21}$ cluster presented lower energy barriers compared to Pd_{43}, which confirmed the favorable impact of PdCo NPs in promoting the dehydrogenation of FA.

Tamarany et al. studied the preparation of PdNi alloys supported in N-doped carbons to evaluate the optimal Pd:Ni ratio, as well as reaction conditions [74]. The N-doped carbon (N-C) was obtained by mixing dicyanoamide with carbon black at 100 °C and then pyrolyzing at 550 °C for 4 h in a N_2 flow. The Pd_1Ni_x alloys supported on N–C (Pd_1Ni_x/N–C) were prepared by dispersing N-C into aqueous solutions containing the metal precursors (i.e., $Pd(NO_3)_2{\cdot}2H_2O$ and $Ni(NO_3)_2{\cdot}6H_2O$) at different Pd/Ni mole ratios. The resulting products were reduced under a H_2/N_2 flow (20% H_2) at 450 °C for 4 h, leading to Pd_1Ni_x/N–C. The catalytic activity for FA dehydrogenation was assessed at 30 °C with FA:SF solution in 1/1 molar ratio for 3 catalysts with different Pd/Ni ratios. The results showed a volcano-type behavior in which the maximum catalytic activity for $Pd_1Ni_{1.3}$/N–C produced a TOF value of 447 h^{-1}. In another experiment, the influence of temperature on the dehydrogenation activity with $Pd_1Ni_{1.3}$/N–C was studied, obtaining an initial TOF value of 4804 h^{-1} at 65 °C. This value could be attributed, in part, to the fact that the sodium formate can potentially react with water to produce H_2 ($HCOONa + H_2O \rightarrow NaHCO_3 + H_2$), particularly at temperatures higher than 65 °C. Furthermore, the

formation of PdNi alloys was confirmed by (a) elemental mapping of $Pd_1Ni_{1.3}$/N–C, using HAADF-STEM, according to the overlap in the positions of Pd and Ni and (b) by the shift to lower binding energies in the Pd 3d spectra, obtained using XPS.

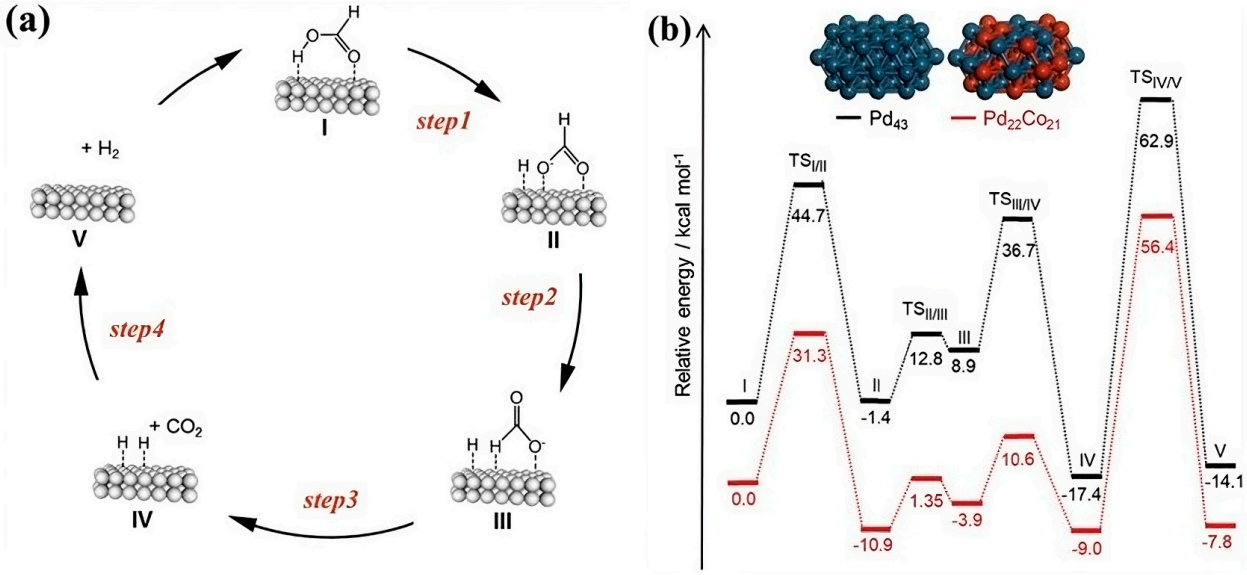

Figure 5. (**a**) Possible reaction pathway; (**b**) potential energy profiles of FA dehydrogenation over Pd_{43} and $Pd_{22}Co_{21}$ cluster models. TSs represent the transition states and I-V the reaction intermediates. Reprinted with permission from [73].

Mori et al. investigated PdCu alloy NPs supported on a macroreticular basic resin with -$N(CH_3)_2$ groups to examine the formation of PdCu alloys and their interactions with the basic groups in the support [75]. The incorporation of both Pd and Cu into the alkaline resin was carried out through a straightforward ion exchange process from an aqueous solution of $PdCl_2$ and $CuNO_3{\cdot}3H_2O$, and later, the samples were reduced by $NaBH_4$. The EXAFS analysis revealed the presence of heteroatomic Pd-Cu bonding. The formation of PdCu NPs with an average size of 1.9 nm was confirmed with TEM. The catalytic activity results measured for the different Pd/Cu molar ratios showed a volcano-type trend, in which the Pd50Cu50's composition presented the maximum TOF value of 810 h^{-1} at 75 °C using an FA/SF 9:1 aqueous solution. The enhancement in the catalytic activity observed in the bimetallic PdCu catalyst compared to the monometallic Pd catalyst can be attributed to the efficient transfer of electrons from Cu to Pd, facilitated by their difference in ionization potential (Cu 7.72 eV and Pd 8.34 eV). Furthermore, the research evidences the substantial influence of the resin's basicity on cleaving O-H bonds. The introduction of Cu is demonstrated to affect the rate-determining step, specifically the C-H bond's dissociation from the metal–formate intermediate, owing to the creation of electron-rich Pd species.

Pd-based trimetallic catalysts have not been as extensively studied as bimetallic catalysts, but they are an interesting alternative for achieving a Pd content reduction and modulating the electronic properties of Pd species.

Yurderi et al. designed carbon-supported trimetallic PdNiAg NPs as catalysts for FA dehydrogenation to study the effect on the catalytic activity of alloying Pd with Ag and Ni simultaneously [76]. The preparation of the catalysts was achieved using the wet impregnation method with a reduction step, and the precursors of the metals were mixed at different molar ratios with the commercial activated carbon. The morphology and size of the PdNiAg/C NPs were studied using TEM, obtaining a good dispersion and with an average particle size of 5.6 nm. The XPS spectra showed the presence of metallic NPs and, also, oxidized species, such as PdO, NiO, $Ni(OH)_2$, NiOOH, and Ag_2O. Among the different compositions studied, the $Pd_{0.58}Ni_{0.18}Ag_{0.24}$/C catalyst showed the best catalytic activity, reaching a TOF of 85 h^{-1} at 50 °C in a 1:1 FA/SF solution. The reusability of that

catalyst was studied after five consecutive cycles of reaction, demonstrating that 94% of the initial catalytic activity was retained.

Wang et al. prepared NiAuPd alloy supported on a commercial carbon in order to investigate this trimetallic composition in comparison with the bimetallic and monometallic catalysts [77]. The synthesis of the catalysts was carried out with a co-reduction method without any surfactant at 25 °C. The images obtained with HAADF-STEM showed that Ni, Au, and Pd were homogeneously distributed in each particle, highlighting that the alloy structure was, indeed, formed. The catalytic activity results for $Ni_{0.40}Au_{0.15}Pd_{0.45}/C$ unveiled a TOF of 12.4 h^{-1} (calculated on the basis of the total amount of metal) at 25 °C and in a pure FA solution without additives.

Dong et al. tailored a system based on PdCoNi NPs supported on N-CN, which was used to study this new composition and the effect of doping with N [78]. N-CN was prepared using a combination of CN and 3-aminopropyl triethoxysilane. The catalysts based on the PdCoNi NPs were synthesized with a coreduction method. Ultrafine NPs were obtained for the $Pd_{0.6}$ $Co_{0.2}Ni_{0.2}$/N-CN catalyst with an average size of 1.6 nm. The XPS analysis detected electron transfer from Co and Ni to Pd, indicating the formation of a solid solution structure of $Pd_{0.6}Co_{0.2}Ni_{0.2}$ NPs, and the presence of pyrrolic N was also detected. The catalytic activity of $Pd_{0.6}Co_{0.2}Ni_{0.2}$/N-CN was measured at 25 °C in a 1:1 aqueous FA/SF solution, obtaining an initial TOF value of 1249 h^{-1}.

Liu et al. performed a study based on a trimetallic AuPdIr nanoalloy supported on N-doped reduced graphene oxide (N-GO) to achieve a catalyst with long-term stability after modulating the electronic properties of the catalyst by the formation of AuPdIr nanoalloy [79]. AuPdIr catalysts were prepared using a coreduction method and by mixing the metal precursors with an APTS/GO solution, obtaining $Au_{0.35}Pd_{0.5}Ir_{0.15}/NH_2$-N-rGO. By XPS, electron transfer from Pd and Ir to Au was observed, which is consistent with their electronegativity (Au 2.4, Pd 2.2, and Ir 2.2), thus confirming the nanoalloy's formation. The performance in FA dehydrogenation was tested, obtaining a TOF value of 12,781.2 h^{-1} at 25 °C in a pure FA solution (Figure 6A), and the temperature increase to 60 °C resulted in a TOF value of 36,598.4 h^{-1}. The recycling stability of $Au_{0.35}Pd_{0.5}Ir_{0.15}/NH_2$-N-rGO was assessed by introducing an additional aliquot of FA after completing the previous cycle, demonstrating excellent stability over 10 reaction cycles. To extend the evaluation to long-term stability, a 150-day experiment was performed. As depicted in Figure 6D, the catalyst retained the ability to catalyze 100% of the FA dehydrogenation for 7.08 min at room temperature, even after 150 days. According to the DFT calculations, this robust activity is ascribed to the incorporation of the high-surface-energy element iridium (Ir), which alters the initial adsorption configuration of HCOOH* and improves the overall performance of the reaction.

As can be extracted from the studies revisited in this section, important efforts have been devoted to achieving high-performing catalysts for the dehydrogenation of FA, which encompass the analysis of properties of the active phase, such as the size of the nanoparticles and their electronic properties, as well as the modification of the carbon support by incorporating heteroatoms, such as nitrogen. The catalysts studied are usually synthesized using well-established protocols, such as impregnation of the supports with metal salts, but other more complex approaches, such as the polyol method, have also been used. It has been found in numerous studies that the use of bimetallic and multimetallic catalysts is a useful approach to synthesizing promising catalysts since the additional metal or metals incorporated into the Pd-based nanoparticles may modify the electronic properties of the Pd active centers, which may alter somehow their performance in the reaction steps involved in the dehydrogenation of FA. In this sense, in the reaction mechanism accepted for that reaction, the role of electron-rich and electron-deficient Pd species is claimed. Such a reaction mechanism encompasses the following steps: (1) adsorption of formate ions on the surface of Pd nanoparticles, which could be favored by the presence of electron-deficient Pd species; (2) cleavage of the C−H bond of the adsorbed formate ion, which is favored by

electron-rich Pd species; and (3) release of H_2 and the regeneration of the catalyst [80,81]. The reaction mechanism is schematized in Scheme 1.

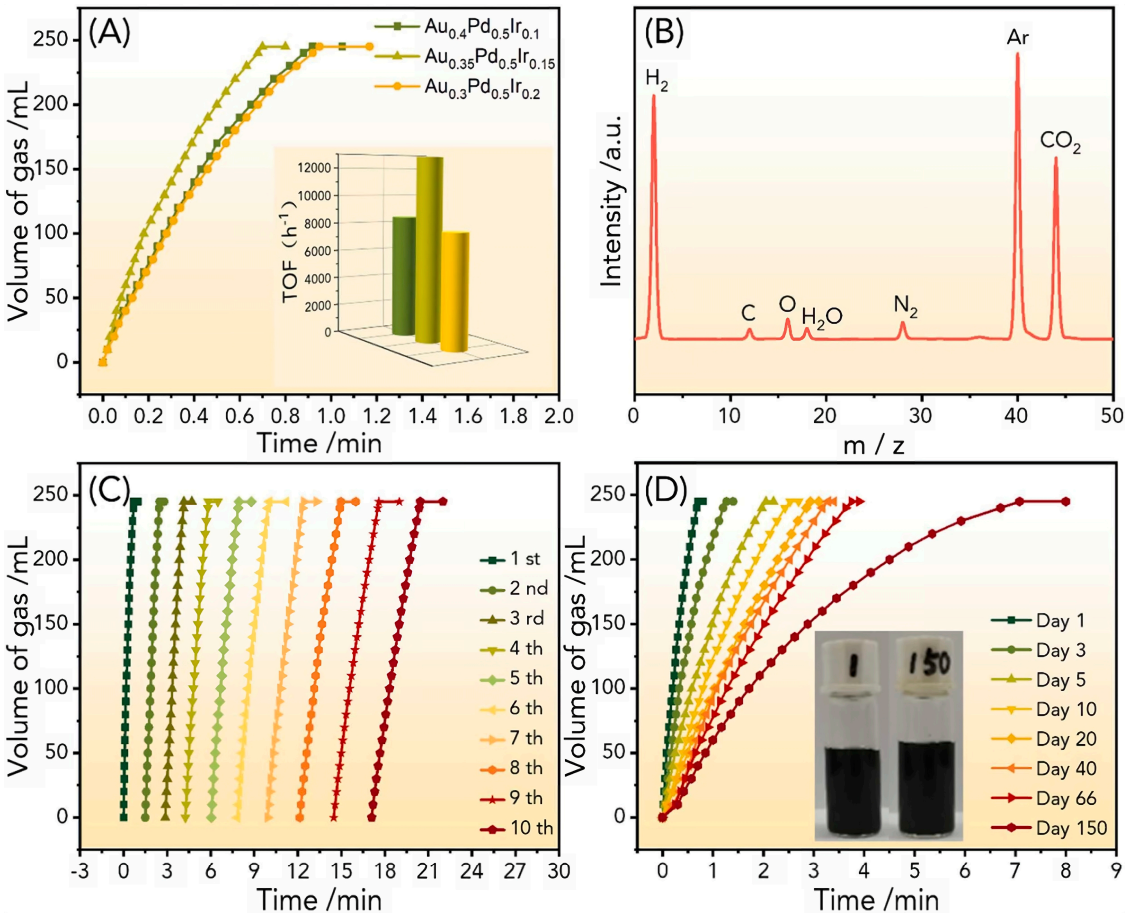

Figure 6. (**A**) Gas generation from FA dehydrogenation at 298 K, with the corresponding TOF values shown in the inset; (**B**) mass spectrometry of released gas from the dehydrogenation of FA over $Au_{0.35}Pd_{0.5}Ir_{0.15}/NH_2$-N-rGO; (**C**) continuous recycling tests and (**D**) 150-day long-term recycling test of $Au_{0.35}Pd_{0.5}Ir_{0.15}/NH_2$-N-rGO in H_2 generation from FA solution, and in the inset is a photo of the catalysts dispersed in the reaction solution on the 1st and 150th day. Reprinted with permission from [79].

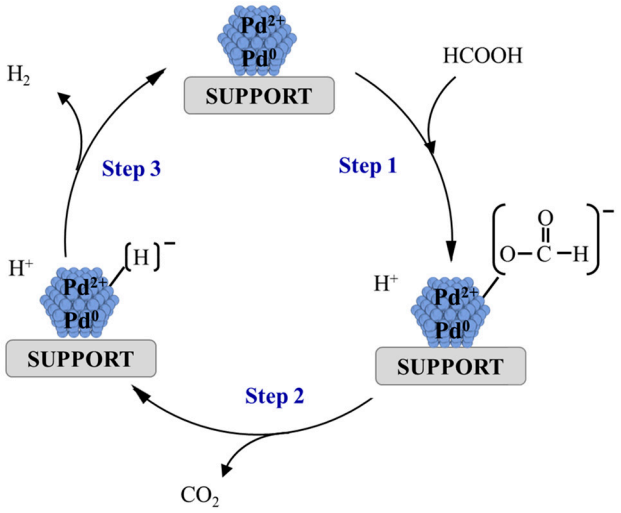

Scheme 1. Simplified reaction mechanism for the production of H_2 from FA.

To summarize the studies reviewed in this section, Table 1 compiles the details of representative Pd-based carbon-supported catalysts.

Table 1. Pd-based carbon-supported heterogeneous catalysts for the dehydrogenation of FA.

Catalyst	Aim of the Study	Pd Loading (wt %)	T (°C)	Additive	Conversion (%)	Selectivity (%)	Reference
Pd/C	Effect of NPs' size	2.3	25	SF	92	-	[49]
Pd/C(3)	Effect of NPs' size	0.4	30	-	-	100	[51]
Pd/N-HTC (n.r.)	Incorporation of N groups	0.7	75	SF	-	-	[53]
Pd/HTNC-950	Incorporation of N groups	4.7	30	SF	-	-	[59]
Pd/N-C	Incorporation of N groups	8.5	45	SF	100	-	[61]
Pd/NHPC-AC	Incorporation of N groups	2.7	60	SF	-	-	[62]
Pd/NH_2-TPC	Incorporation of N groups	2.0	60	-	100	100	[54]
Pd/N-CM	Incorporation of N groups	1.0	149	-	50	50	[63]
Pd/hatnCTF	Incorporation of N groups	1.0	180	-	-	>99	[64]
Pd1Ag2	Incorporation of other metal	0.5	30	SF	-	100	[44]
Pd_7Ag_3/CNT	Incorporation of other metal	-	30	SF	-	-	[68]
Ag_1@Pd_1/N-GCNT	Incorporation of other metal	9.7	25	-	100	100	[69]
PdAg/N-AS	Incorporation of other metal	0.8	75	SF	-	-	[70]
AuPd/n-CNS-T_h-160	Incorporation of other metal	-	25	SF	-	100	[71]
Pd_1Au_1/72-LA	Incorporation of other metal	2.7	60	-	-	-	[72]
PdCo/g-C_3N_4	Incorporation of other metal	1.0	75	SF	-	100	[73]
$Pd_1Ni_{1.3}$/N–C	Incorporation of other metal	1.0	65	SF	-	-	[74]
$Pd_{50}Cu_{50}$/resin 1	Incorporation of other metal	-	75	SF	-	100	[75]
$Pd_{0.58}Ni_{0.18}Ag_{0.24}$/C	Incorporation of other metal	0.6	50	SF	100	100	[76]
$Ni_{0.40}Au_{0.15}Pd_{0.45}$/C	Incorporation of other metal	0.4	25	-	70	100	[77]
$Pd_{0.6}$ $Co_{0.2}Ni_{0.2}$/N-CN	Incorporation of other metal	0.6	25	SF	99	100	[78]
$Au_{0.35}Pd_{0.5}Ir_{0.15}$/$NH_2$-N-rGO	Incorporation of other metal	0.5	25	-	100	100	[79]
Pd/mpg-C_3N_4	Effect of the support	9.5	55	-	-	-	[82]
Pd/r-GO	Effect of the support and reaction conditions	1.0	80	HCOOK	96.6	-	[83]
Pd/PDMC-800-16	Incorporation of N groups	-	80	SF	-	-	[84]
PdAg/amine-MSC	Incorporation of other metal	1.0	75	SF	-	>99	[55]

3. Hydrogenation of CO_2 to FA

The hydrogenation of CO_2 to FA is more challenging than the reverse reaction, the dehydrogenation of FA, but this reaction is essential for obtaining a hydrogen charge–discharge system and achieving a carbon-neutral cycle. This process is thermodynamically unfavorable, as the net reaction involving gaseous CO_2 and H_2 to form liquid HCOOH is endergonic, primarily due to the significant entropic contribution (ΔG_{298K} = 32.9 kJ·mol^{-1}) [85,86]. A notable challenge in this process lies in activating the chemically stable CO_2 molecule, with a linear molecular structure (O=C=O) and a high bond energy of 806 kJ mol^{-1} [86,87]. Therefore, the application of external energy is required in addition to suitable catalysts with high selectivity. Among the investigated heterogeneous catalysts, Pd-based catalysts have undergone extensive research and frequently display notable activity, surpassing other transition metals in the hydrogenation of CO_2 to formic acid/formate. This superiority stems from their high stability under acidic or basic reaction conditions and a strong affinity for H_2 spillover [88]. In particular, catalysts based on Pd NPs supported

on carbon materials stand out for the modulation of their textural properties and ease of heteroatom incorporation.

To strategically formulate carbon-supported Pd-based catalysts for the hydrogenation of CO_2 into formate/formic acid, it is essential to identify the key factors impeding catalytic performance. As previously stated, this reaction faces thermodynamic challenges, primarily arising from the transition from the gaseous phase (H_2 and CO_2) to liquid products, necessitating a substantial positive change in the Gibbs free energy [89,90]. The most direct approach to overcome the thermodynamic constraint is to conduct the reaction in the liquid phase (such as with water, alcohol, DMSO, and ionic liquids) [91]. The reaction experiences a slight exothermal shift attributed to the solvation effect (see reaction 3) [27,92]. Moreover, the hydrogenation of CO_2 gains increased advantages through the inclusion of base additives in reaction solutions (such as amines, bicarbonates, and hydroxides), effectively impeding the reverse reactions (dehydration/dehydrogenation of FA) [27]. Certainly, the hydrogenation of CO_2 into formic acid/formate is affected by several factors, including the pH of the solution, type of base, reaction temperature, and the pressures of H_2 and CO_2.

$$CO_2(aq) + H_2(aq) \rightarrow HCOOH(aq), \ \Delta G^{\circ}{}_{298K} = -4.0 kJmol^{-1} \quad (3)$$

As previously mentioned, the hydrogenation of CO_2 into FA/formate typically occurs under alkaline conditions, necessitating that the catalyst possess alkali-resistant properties. Nevertheless, Pd NPs tend to aggregate into larger particles or leach into the solution during the catalytic reaction process [90]. This underscores the importance of safeguarding Pd atoms as a critical factor in attaining high catalytic performance. To date, multiple approaches, including the anchoring of functional groups (nitrogen groups) on supports or Pd NPs [82,84,93–95], alloying Pd NPs with other transition metal atoms [55,96–98], confining the Pd NPs within pores or cavities of the supports [96,97], and modification of surface area have been employed to address the challenges associated with the catalytic hydrogenation of CO_2 to produce FA/formate.

Regarding the experimental conditions used in the hydrogenation of CO_2, the typical setup is a stainless-steel autoclave batch reactor, which is pressurized and heated, in which the catalyst is normally mixed with water. Mainly, in the studies reported in the literature, two experimental methods can be differentiated. The first does not use an additive base: exclusively H_2 and gaseous CO_2 are used for the hydrogenation. In this case, more severe reaction conditions are usually required to obtain an adequate conversion of CO_2 into formate. In the second case, base additives, such as $NaHCO_3$, $KHCO_3$, and NH_4HCO_3, are used to promote the course of the reaction; in this way a quantity of CO_2 is initially in the liquid phase, which facilitates the interaction with the catalyst [27,91,92]. Concerning the temperature and total pressure used, different values can be found, including temperatures between 25 and 150 °C and pressures between 4 and 80 MPa [99,100]. To ensure an adequate catalytic performance, the reaction is allowed to proceed for several hours, normally reaching 24 h. The products in the liquid phase are then analyzed using HPLC to check that formic acid/formate is obtained.

Herein, the most significant work on the hydrogenation of CO_2 to FA/formate attained by carbon-supported Pd-based catalysts will be revisited.

3.1. Carbon-Supported Monometallic Pd Catalysts

Since the hydrogenation of CO_2 into FA/formate is a more challenging reaction than the reverse reaction, studies are needed to modulate the experimental conditions and catalyst properties to obtain better catalytic activity and to gain insight into the reaction's mechanism.

Su et al. investigated the reaction conditions for the hydrogenation of bicarbonates into CO_2 over Pd catalysts [101]. First, bicarbonate and carbonate salts were compared with different cations (Na^+, K^+, and NH_4^+) for hydrogenation. It was found that the bicarbonate salts presented better activity for hydrogenation, specifically NH_4HCO_3. For the study of

the hydrogenation reaction with an aqueous solution of NH_4HCO_3 at pH 7.7 using a Pd/AC catalyst, an ammonium formate yield of 59.6% was obtained with a turnover number (TON) of 1103 after reaction for 1 h and with an initial H_2 pressure of 5.5 MPa. Considering that the hydrogenation of aqueous NH_4HCO_3 involves multiple phases (i.e., gas, liquid, and solid), the diffusion of the reactant, H_2, might be the rate-limiting step due to its low solubility in water. Activated carbon, typically a hydrophobic support, is capable of storing H_2. H_2 may be concentrated locally within the carbon channels or on the surface of the carbon support, facilitated by H_2 spillover from the Pd metal. A ^{13}C NMR analysis confirmed that the cations of the bicarbonate salts influenced the equilibrium between carbonate and bicarbonate ions, with NH_4HCO_3 exhibiting the highest concentration of HCO_3^- in the aqueous solution, resulting in the highest formate yield of the hydrogenation reaction. Furthermore, the effect of the reaction temperature was studied, and it was observed that the highest formate yield was achieved at room temperature. This suggests that under these conditions for the hydrogenation of bicarbonates, additional external energy is not required. The ammonium formate dehydrogenation reaction was studied at 80 °C, obtaining a H_2 yield of 92.1% with a TON of 1698 after 1.5 h of reaction.

Shao et al. prepared Pd-based nanocatalysts supported on mesoporous carbon nitride (mgp-C_3N_4) for the hydrogenation of bicarbonate to formate to study the influence of the support, as well as the reaction conditions [93]. mgp-C_3N_4 was obtained using dicyandiamide and a silica template by the pyrolysis treatment. The catalysts, Pd/mgp-C_3N_4 and a Pd/AC, were obtained using the wet chemical reduction method. The images obtained by TEM show that the Pd NPs were well dispersed on the two supports, with an average particle size of 1.9 nm for Pd/mgp-C_3N_4 and 2.4 nm for Pd/AC. The XPS analyses indicated that the N species primarily comprised sp^2 hybridized aromatic N bonded to carbon atoms in the form of C=N-C and tertiary N bonded to carbon atoms (N-$(C)_3$), and a small number of NH groups were observed. In addition, the Pd 3d XPS analysis showed the presence of Pd^0 and Pd^{2+}. The hydrogenation reaction was studied from 50 to 80 °C, with $p(H_2)$ = 6.0 MPa, 20 mmol $KHCO_3$, and 5 mL H_2O. Since the hydrogenation of bicarbonate ions is exothermic, the rising temperature caused an increase in the reaction rate, but the final concentration of formate decreased as a result. The TOF values calculated at 80 °C for Pd/mgp-C_3N_4 and Pd/AC were 5926 and 4672 h^{-1}, respectively. In the study, it was proposed that the primary or secondary amino groups on the surface of mpg-C_3N_4 could facilitate the activation of HCO_3^- and enhance the hydrogenation of bicarbonate. The reusability of Pd/mgp-C_3N_4 was tested for six cycles, showing high stability in the reaction. In that work, the observation that only formate was formed as a product suggested that the hydrogenation occurred via the insertion mechanism. With this mechanism, which is shown in Figure 7, in an initial stage HCO_3^- can be easily adsorbed on the surface of the catalyst by the formation of O-H···N. Subsequently, active hydrogen is generated over Pd NPs, initiating an attack on the positively polarized carbon in HCO_3^-, resulting in the simultaneous formation of the formate intermediate, the release of the produced HCO_2^-, and the adsorption of a new HCO_3^- anion.

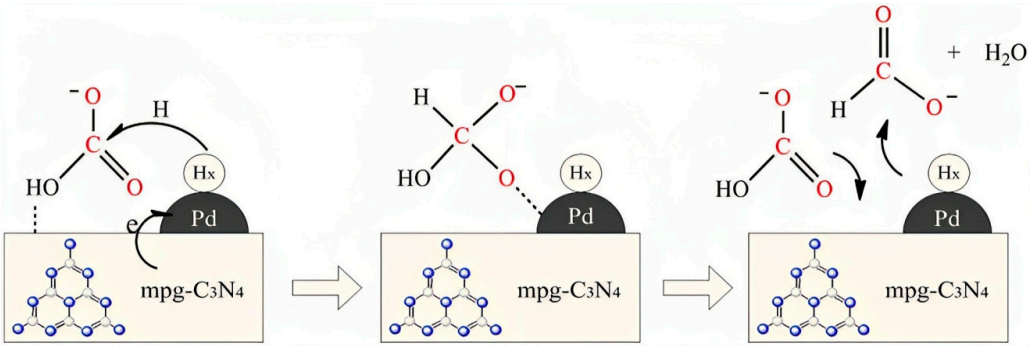

Figure 7. Possible mechanism of the reaction of bicarbonate hydrogenation over Pd/mpg-C_3N_4. Reprinted with permission from [93].

Zhou et al. prepared Pd catalysts supported on *g*-C_3N_4 modified via the addition of a Schiff base, terephthalaldehyde (TPAL), to study its effect on the catalytic activity in the hydrogenation of CO_2 into formate [102]. The synthesis of the support (u-CN_{100}) was carried out by mixing urea and TPAL and then heating it at 550 °C in a muffle; then, Pd/u-CN_{100} was obtained with the impregnation approach. The CO_2 hydrogenation experiments were performed in the aqueous phase consisting of ethanol (15 mL) and triethylamine (Et_3N) at 110 °C, with a total pressure of 7 MPa (H_2/CO_2 1:1). The catalytic activity results showed a great improvement in the TOF value when TPAL was added, obtaining 98.9 h^{-1}, while for Pd/u-C_3N_4 (without TPAL) the TOF value was 14 h^{-1}. The stability of Pd/u-CN_{100} was studied after five consecutive cycles after which the catalyst was collected and did not show a remarkable loss of activity. That marked stability may be related to the Pd species anchored to the support by the N groups. The presence of Pd nanoclusters was observed by TEM, with an average particle size for Pd/u-CN_{100} of 1.57 nm and for Pd/u-C_3N_4 of 2.22 nm. Moreover, the XPS analysis showed a higher proportion of Pd^{2+} species in the Pd/u-CN_{100} than in the Pd/u-C_3N_4, confirming, again, the stronger interaction with N species. Thus, the addition of a Schiff base resulted in a catalytic improvement due to the modulation of the electronic properties of Pd species, as well as the anchoring effect on these species.

Wang et al. designed a palladium-based system supported on N-doped mesoporous carbon (NMC) as a bifunctional catalyst for formate-mediated hydrogen storage [94]. NMC was prepared with the hard templating method using mesoporous silica as a template and carbonized under ammonia flow for nitridation. Palladium-supported catalysts were prepared using the wet chemical reduction method. The catalytic performance of bicarbonate hydrogenation for Pd/NMC-8 (nitridation treatment at 873 K) obtained a turnover number (TON) of 1598 at 80 °C in 2 h and a conversion of 69.7% in aqueous $KHCO_3$ solution and with a H_2 pressure of 6 MPa. The reusability of the catalyst was measured after 4 runs, in the fourth run the formate yield decreased by 13.3%. Bicarbonate hydrogenation was studied for Pd/NMC-8 at 80 °C obtaining a TOF in the first 10 min of 2416 h^{-1} in a HCOOK aqueous solution. The average particle size obtained for the Pd NPs in Pd/NMC-8 by STEM was 2.4 nm, which was smaller than for the catalyst without N groups. The XPS analysis detected pyridine, nitrile, pyrrole, and quaternary N species. In addition, a higher contribution of Pd^{2+} was detected in the N-doped support, demonstrating the interactions between the nitrogen species and Pd NPs. That work demonstrates how the nitrogen groups in the support play a crucial role in promoting the bicarbonate/formate redox equilibrium.

Song et al. prepared catalysts based on Pd NPs supported on chitin using the wet impregnation method followed by reduction to investigate the effect of the interaction of chitin with Pd sites [95]. The morphology of the Pd/chitin was determined by SEM, yielding a fiber form, and some of them were disorderly gathered to form a flowerlike architecture. The SEM analysis revealed that the Pd NPs were well distributed in the chitin fibers and the average particle size was 1.84 nm. The analysis of the Pd 3d XPS spectra showed the presence of Pd^0 and $Pd^{\delta+}$; the oxidized species were attributed to the electronic donation of Pd to the acetoamide nitrogen groups of chitin. Thus, the interaction of the acetoamide groups of chitin with Pd was confirmed. The CO_2 hydrogenation reaction was carried out in an aqueous solution using Na_2CO_3 as an additive under a total pressure of 4 MPa and at 60 °C. Under these conditions, Pd/chitin with 0.25% Pd content obtained the highest TOF value, 257 h^{-1}. The recyclability study showed good stability after five reaction cycles.

Some other studies report the ability of the developed materials to catalyze both the dehydrogenation of FA and the hydrogenation of CO_2 or bicarbonates. For example, Lee et al. designed a system based on Pd NPs supported on mpg-C_3N_4 for H_2 generation and storage via FA dehydrogenation and CO_2 hydrogenation [82]. The Pd NPs were immobilized onto mpg-C_3N_4 using the wet impregnation method with H_2 reduction. The Pd NPs were observed to be uniformly distributed, with an average size of 1.7 nm, as

evidenced by HRTEM. Pd/mpg-C_3N_4 achieved a TOF for the FA dehydrogenation reaction of 324 h^{-1} at 55 °C, in an aqueous phase without any additives. For investigating the CO_2 hydrogenation reaction, in which FA can react with H_2 to produce products like methanol and methane, Et_3N was employed to capture the formed FA. The overall gas pressure was maintained at 40 bar, with adjustments made by heating the mixture to 100 °C and 150 °C. The amount of FA formed depended on the reaction conditions. It was found that a decrease in the CO_2 pressure did not noticeably affect FA production, while the activity decreased when the H_2 pressure was low. It was also observed that the activity improved when the temperature increased. The results obtained by ^{13} C NMR, after an experiment in which CO_2 was pressurized in a reactor containing Et_3N and deuterium, verified the formation of Et_3N-CO_2. The highest activity was observed by employing CO_2 and H_2 pressures of 13 bar and 27 bar, respectively, at a temperature of 150 °C, resulting in the production of 4.74 mmol of FA.

Bi et al. designed a system for the development of a formate-based hydrogen battery mediated by Pd catalysts supported on reduced graphene oxide (r-GO) [83]. Pd/r-GO was synthesized using a one-step coreduction method. The TEM images showed spherical and uniform Pd particles with a mean size of 2.4 nm dispersed on the r-GO sheets. The predominant presence of Pd^0 on the r-GO was confirmed by XPS analysis. The underlying support surface may cause a structural effect to occur on the electronic structure of Pd, creating a lattice microstrain, which could be related to a higher activity in the dehydrogenation of formate. This fact was confirmed by XRD of the Pd/r-GO. The dehydrogenation reaction was studied at 80 °C in an aqueous solution of 5 mL HCOOK 4.8 M; under these conditions, Pd/r-GO with 1 wt% Pd achieved a TOF value of 11,299 h^{-1}. The hydrogenation reaction to potassium formate was performed in the same aqueous solution, and with a total pressure (H_2/CO_2 1:1) of 80 bar at 100 °C, the Pd/r-GO catalyst reached a TON value of 2420, and an almost complete conversion was achieved in 10 h. In view of the good catalytic results, cyclical operation tests were carried out by coupling the two reactions. Consequently, alternating pressurized charging (hydrogenation reaction) and pressure-free discharging (dehydrogenation reaction) steps were implemented to assess the feasibility using a commercially standard autoclave. The assessment was performed during six consecutive, identical cycles of H_2 release, and the hydrogenation of the resulting $KHCO_3$ was accomplished.

Koh et al. synthesized small Pd NPs supported on mesoporous N-doped carbon (PDMC) for hydrogen storage and release based on bicarbonate/formate [84]. The N-doped support was prepared with a PANI-assisted method using silica as a template. The resulting material was pyrolyzed in an Ar atmosphere; then, the product was treated with NaOH solution in an autoclave at 100 °C for 18 h to remove the silica template. Catalysts with the formula Pd/PDMC-T-x (where *T* represents the pyrolysis temperature, and *x* represents the amount of colloidal silica template) were prepared using the wet impregnation method followed by a reduction in the N_2/H_2 atmosphere. The average particle size measured by TEM for Pd/PDMC-800-16 was 1.6 nm, proving that the use of colloidal silica templates indirectly helped to obtain small NPs. The dehydrogenation reaction of formate was carried out in a 5 mL 1 M aqueous solution of HCOONa at 80 °C. The highest catalytic activity was obtained for the catalyst Pd/PDMC-800-16, obtaining a TOF value of 2562 h^{-1}. Additionally, it was observed that the catalytic activity of the catalysts followed a volcano-like trend with the pyrolysis temperature, reaching a maximum when the temperature was 800 °C. Furthermore, the reusability study, measured for three cycles, demonstrated the stability of the catalyst. The hydrogenation reaction of sodium bicarbonate was performed in a 1 M aqueous solution of $NaHCO_3$, with a H_2 pressure of 40 bar and at 80 °C. Under these conditions, Pd/PDMC-800-16 presented the best activity, with a TON value of 1625. The surface chemistry of the catalysts was studied by XPS, and the presence of pyridinic-N, pyrrolic-N, quaternary-N, and pyridinic-N^+-O^- groups was detected. In Pd/PDMC-800-16, higher concentrations of pyrrolic-N and pyridinic-N were identified. The EXAFS study revealed that the coordination numbers (CNs) of the Pd-Pd bonding in all of the Pd/PDMC-

T-x materials (CN Pd-Pd ≈ 2 to 4) were significantly lower than that of the bulk Pd foil (CN Pd-Pd ≈ 12). This affirmed the presence of well-dispersed Pd nanoclusters, consisting of only a few atoms, on the nitrogen-doped carbon support materials.

3.2. Carbon-Supported Multimetallic Pd-Based Catalysts

For CO_2 hydrogenation, there are not many studies in which multimetallic catalysts were used. However, alloying Pd with other metals could be an interesting option, since pure Pd can be easily poisoned by some reaction intermediates such as CO [103,104].

Yang et al. investigated the encapsulation of PdAg alloy NPs in N-doped microporous hollow carbon spheres (NMHCS) to protect the NPs and also to improve the mass transfer for the hydrogenation of CO_2 into formate [96]. The NMHCS were prepared using ethylenediamine as the nitrogen source and SiO_2 as the template. The catalysts were prepared using the impregnation–reduction method to form PdAg@NMHCS spheres. The FE-SEM images show uniform spheres without impurities. It was observed by TEM that PdAg@NMHCS-0.6-500 (carbonized at 500 °C) presents hollow cavities with an approximate diameter of 340 nm and a N-doped carbon shell of 30 nm in thickness. The PdAg NPs have an average size of 7.5 nm and are uniformly encapsulated in the hollow cavities. The presence of PdAg alloy was confirmed using STEM elemental maps. The N 1s orbital spectra, determined by XPS, showed that with an increase in the carbonization temperature from 400 to 500 °C, the ratio of N-pyrrole/N-pyridinic increased. That means that part of the N-pyridinic was transformed into N-pyrrole at 500 °C. The hydrogenation reaction of CO_2 into formate was carried out using a 15 mL aqueous solution of 1.0 M $NaHCO_3$ at 100 °C and a total pressure of 2.0 MPa (H_2/CO_2 1:1). For PdAg@NMHCS-0.6-500, TON values of 640 and 2750 were obtained after 2 and 24 h, respectively, presenting a better catalytic activity than the catalyst without a hollow structure, indicating that this structure plays an important role in achieving high catalytic activity. In addition, the reaction was studied using other bases, such as NaOH, NH_4HCO_3, and Na_2CO_3, and only H_2O. The best result was obtained for $NaHCO_3$, and the use of only pure water resulted in a sharp decline in activity. This fact shows that alkaline solutions facilitate the absorption of CO_2 in solution for the formation of HCO_3^-.

Masuda et al. prepared a catalyst based on PdAg NPs supported on phenylamine-functionalized mesoporous carbons (MSCs) to study the effect of the presence of phenylamine groups for FA and CO_2 interconversion [55]. The MSCs were treated with an aqueous nitric acid solution and then functionalized with p-phenylenediamine to produce amine-MSCs (see Figure 8). The PdAg-based catalysts were prepared using the impregnation method with the supports and subsequent reduction with $NaBH_4$. Good dispersion of the Pd and Ag NPs was observed with an average size of 1.2 nm, measured by HAADF-STEM. The slight shift in the XPS spectra toward lower binding energies for the 3d Pd peaks in PdAg/amine-MSCs compared to PdAg/MSCs demonstrated that the amine groups affected the electronic states of Pd, confirming their interaction. In addition, PdAg alloying could also be verified by XPS and EXAFS. The EXAFS results clarified that in PdAg/amine-MSCs, the Ag atoms are predominantly situated in the core region, while the Pd atoms are positioned in the shell. The FA dehydrogenation reaction was measured in an aqueous FA/SF solution in a 9:1 molar ratio at 75 °C; for the PdAg/amine-MSC catalyst, a TOF value of 5638 h^{-1} was obtained considering the total amount of Pd. The hydrogenation of CO_2 to form FA was assessed with an aqueous $NaHCO_3$ solution under a total pressure of 2 MPa (H_2:CO_2 = 1:1, volume ratio) at 100 °C, and the PdAg/amine-MSCs showed a selectivity > 99% and a TOF and reaction rate of 839 h^{-1} and 328 $mmolh^{-1}g_{Pd}{}^{-1}$, respectively. The DFT-calculated potential energy profiles confirmed that the amine-functionalized catalyst supports both reactions. The graphitized phenylamine group has a positive impact on the O-H bond dissociation during the dehydrogenation of formic acid, while the interaction between HCO_3^- and phenylamine molecules plays a crucial role in stabilizing the reaction intermediate in the hydrogenation of CO_2. A catalyst sample was initially employed for the dehydrogenation of FA over

15 min and, subsequently, collected by centrifugation after the reaction. The reversibility of the interconversion between FA and CO_2 was investigated for PdAg/amine-MSCs. The recovered catalyst was then re-dispersed in a 1.0 M aqueous $NaHCO_3$ solution and used for the hydrogenation reaction to generate formic acid. After 24 h, the catalyst was collected through centrifugation, re-dispersed, and utilized once more for the dehydrogenation of FA. The reversibility of FA and CO_2 interconversion was assessed for PdAg/amine-MSCs. The catalyst reversibility was confirmed over three consecutive cycles, demonstrating no inherent loss of catalytic activity.

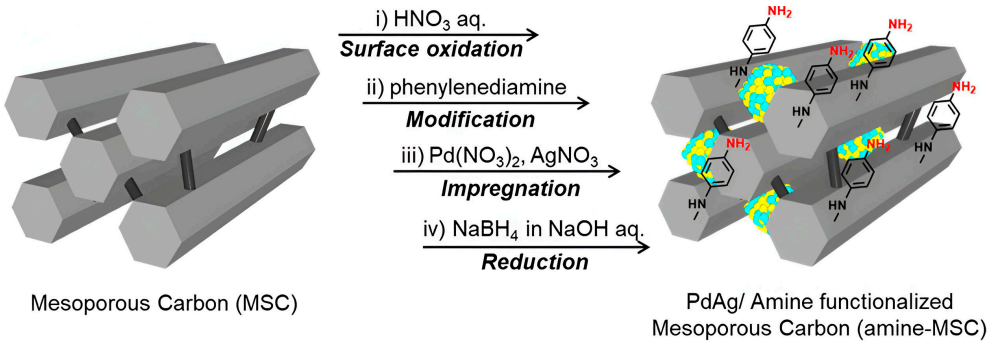

Figure 8. Scheme of PdAg/amine-MSC synthesis. Reprinted with permission from [55].

Yang et al. prepared PdCu alloy NPs confined in mesoporous hollow carbon spheres (MHCS) to protect the NPs from sintering for the hydrogenation of CO_2 to formate [97]. The method of preparation of these catalysts was similar to that presented in the previous work of these authors [96]. TEM images show hollow spheres of approximately 220 nm diameter and 40 nm shell thickness. The HAADF-STEM observations for Pd_2Cu_{14}-N@MHCS showed NPs encapsulated within hollow cavities, with an average particle size of 5 nm. The lattice fringes observed in the Pd/Cu nanoparticles are recognized as corresponding to the Cu(111) plane with a lattice spacing of 0.21 nm, suggesting the dispersion of Pd atoms within the Cu nanoparticles. The surface species were determined by XPS, confirming the presence of reduced Cu and Pd, and the electron transfer from Cu to Pd was verified. In addition, it was possible to verify by EXAFS the formation of the PdCu alloy. The hydrogenation reaction of CO_2 into formate was carried out under a total pressure of 2 MPa in an aqueous solution of 1 M $NaHCO_3$ at 100 °C. For the Pd_2Cu_{14}-N@MHCS catalyst, a TON value of 1432 was obtained after 24 h. Furthermore, kinetic investigations were carried out by varying the reaction conditions, which revealed that bicarbonate adsorbs readily on Cu atoms. These studies suggest the following reaction mechanism for this catalyst: (1) adsorption and activation of H_2 on Pd, (2) gaseous CO_2 dissolves in the aqueous solution to form HCO_3^-, (3) HCO_3^- adsorbs on the Cu atoms, (4) nucleophilic hydrogen atom formed on Pd reacts with HCO_3^- adsorbed on Cu, forming formate ion, (5) OH^- adsorbs on MHCS, and (6) H remaining on Pd reacts with OH^- to form H_2O, which regenerates the catalyst. The computational calculations obtained by DFT demonstrated that alloying Cu with Pd facilitates the dissociation of H_2 and also influences the activation energy for the reduction of HCO_3^-.

Nguyen et al. developed a catalyst based on PdNi alloy supported on carbon nanotube–graphene (CNT-GR) to study the Pd-Ni synergistic effect in catalysts with an optimal composition for the hydrogenation of CO_2 to FA [98]. PdNi supported on a CNT-GR composite was obtained using the wet impregnation method followed by reduction. Previously, the optimum composition for these catalysts was found to be Pd_3Ni_7. The PdNi NPs were observed, using TEM, to be uniform and well dispersed, with an average particle size of 4 nm. After the HRTEM analysis, the presence of the alloy was confirmed by PdNi (111) at a lattice spacing of 0.222 nm. The presence of mixed valences for Pd (Pd^0, Pd^{2+}, and Pd^{4+}) could be observed, but the most oxidized species were found in a lower proportion. The CO_2 hydrogenation reaction was carried out for 15 h in an aqueous solution of distilled water without any base additive. When the reaction was studied with Pd_3Ni_7/CNT-GR

at 40 °C and total pressure at 50 bar (H_2/CO_2 1:1), the highest FA yield, 1.93 mmol, was achieved. Furthermore, higher Pd contents, including the monometallic composition, did not result in a better yield, highlighting the synergistic effect of the optimal composition obtained with Pd_3Ni_7. On the other hand, the study of different reaction temperatures revealed that increasing the temperature above 40 °C was counterproductive. This could be explained considering that the reaction between CO_2 and H_2 at high temperatures normally results in the formation of CO and H_2O or the back decomposition of FA. Furthermore, at temperatures below 40 °C, the reaction kinetics were not favorable for overcoming the activation barrier of the reaction. The stability study revealed that after the first cycle, the activity decreased significantly, but the yield stabilized from the second to the seventh cycle, with negligible deactivation.

The studies reviewed in this section demonstrate that great efforts have been made to achieve high-performance catalysts for CO_2 hydrogenation. The different studies conducted to achieve this objective cover the following aspects: (a) study of the reaction conditions (p H_2/CO_2, temperature, and base additives such as $KHCO_3$ and $NaHCO_3$); (b) analysis of the properties of the active phase (composition and electronic properties); and (c) modification of the carbon support (modulation of the textural properties and its surface chemistry by the addition of heteroatoms such as N). The catalysts were prepared using well-known methods, mostly wet impregnation, followed by reduction or coreduction and, in some cases, colloidal synthesis was also used. It was verified in several examples how the use of additives ($NaHCO_3$, $KHCO_3$, etc.) can facilitate the reaction, lowering the high temperatures and pressures required. The incorporation of N groups in the support structure was found to be a good approach to modulating the electronic properties of the catalyst and improving the anchoring of the active phase to the support, thus improving the activity and stability of the catalysts for the hydrogenation of CO_2. Also, the formation of Pd alloys with transition metals of different electronegativity has been of interest because of their ability to modify the electron density of the Pd active centers, resulting in alterations in the catalytic performances. Considering the mechanism of the reaction for CO_2 hydrogenation, a possible general mechanism would involve the dissociative adsorption of H_2 on the Pd surface to form Pd-H species, which then become negatively polarized to drive the hydride transfer to molecular hydride acceptors as bicarbonates, resulting in the generation of formate [84,91,93,94,98,105].

In order to summarize the studies reviewed in this section, in Table 2 is compiled information on the details of various Pd-based carbon-supported catalysts.

Table 2. Pd-based carbon-supported heterogeneous catalysts for the hydrogenation of CO_2.

Catalyst	Aim of Study	Pd Loading (wt %)	T (°C)	p H_2/CO_2 (MPa)	Additive	Conversion (%)	Selectivity (%)	Reference
Pd/AC	Effect of reaction conditions	5.0	20	5.5/-	NH_4HCO_3	59.6	-	[101]
Pd/mgp-C_3N_4	Effect of the support	2.0	80	6/-	$KHCO_3$	-	-	[93]
Pd/u-CN_{100}	Incorporation of N groups	2.8	110	3.5/3.5	EtOH + Et_3N	-	-	[102]
Pd/NMC-8	Incorporation of N groups	4.6	80	6/-	$KHCO_3$	69.7	-	[94]
Pd/chitin	Effect of the support	0.25	60	2/2	-	-	-	[95]
Pd/mpg-C_3N_4	Effect of the support	9.5	150	27/13	Et_3N	-	-	[82]
Pd/r-GO	Effect of the support and reaction conditions	1.0	100	40/40	$KHCO_3$	96.7	-	[83]
Pd/PDMC-800-16	Incorporation of N groups	-	80	40/-	$NaHCO_3$	82	-	[84]
PdAg@NMHCS-0.6-500	Incorporation of other metal	1.0	100	1/1	$NaHCO_3$	-	-	[96]
PdAg/amine-MSC	Incorporation of other metal	1.0	100	1/1	$NaHCO_3$	-	>99	[55]
Pd_2Cu_{14}-N@MHCS	Incorporation of other metal	1.0	100	1/1	$NaHCO_3$	-	>99	[97]
Pd_3Ni_7/CNT-GR	Incorporation of other metal	5.1	40	25/25	-	-	>99	[98]

4. Conclusions

The present review summarizes recent work on heterogeneous Pd-based catalytic systems for hydrogen storage mediated by the HCOOH-CO_2 couple. Given the great relevance that H_2 has acquired as an energy vector in recent years, this topic is of great importance to alleviate the problems related to H_2 production and storage. Extensive research has been conducted on the dehydrogenation of FA, exploring factors such as the significance of the features of the metal active phase and the support, along with the experimental conditions. Moreover, theoretical investigations have been performed to disclose important features for the design of catalysts with high catalytic activity and to obtain information about the reaction mechanism. Among the different heterogeneous catalysts studied, those based on Pd NPs stand out for their high selectivity and conversion in the production of H_2 at moderate temperatures. As for the support, carbon materials are an outstanding option due to their different tailored characteristics and the possibility of including heteroatoms in their structure. Considering the varied properties of the active phase, the pursuit of cost-effective catalysts has led to the exploration of nanoarchitectures for the attainment of a substantial proportion of surface Pd active sites. In addition, it has been evidenced that the incorporation of basic nitrogen functional groups in the support can greatly improve the catalytic activity and stability by different effects: (i) anchoring the Pd NPs in the support; (ii) modifying the electronic properties of Pd species that are involved in the reaction mechanism, improving the rate of the catalytic steps; (iii) interacting with the molecules of FA. The formation of Pd-based multimetallic catalysts through the formation of alloys with the incorporation of one or more metals has also been studied. It has been confirmed that after the formation of alloys with Pd, the electronic properties can be modulated and the resistance to CO poisoning can be improved. Despite all of the improvements that have been implemented to obtain a high performance for this reaction, there are still shortcomings that limit the practical application of large-scale systems. Among these limitations are the use of additives, usually formates (HCOONa or HCOOK), as well as the loss of stability after several reaction cycles. These limitations should be the focus of research for future studies. On the other hand, the hydrogenation of CO_2 to FA/formate on carbon-supported Pd-based catalysts has not been as extensively studied as the reverse reaction due to the unfavorable thermodynamics of the reaction. However, the studies revisited in this review have focused on adjusting the experimental conditions to promote the exothermicity of the reaction and to understand the mechanism of the reaction in order to modulate the properties of the catalysts. The study of CO_2 hydrogenation in aqueous media with additives such as $NaHCO_3$ and $KHCO_3$ has shown an improvement in the course of the reaction due to the decrease in Gibbs energy in the aqueous phase. Concerning the properties of the active metal phase and the support, the same aspects as those considered for the optimization of the performance of the catalysts studied for the dehydrogenation of FA (i.e., particle size reduction, incorporation of another metal, and doping with nitrogen groups) have also resulted in an improvement in the catalytic activity of the catalysts for the hydrogenation of CO_2. Despite the knowledge gained about this reaction, efforts are still needed for the design of catalysts with high activity and stability to allow for the reduction of high temperatures and pressures, as well as the use of base additives.

The objective of future research will be to develop a catalyst with high activity and stability for both reactions and operating under mild conditions. In an ideal scenario, a single system would perform the dehydrogenation and hydrogenation reactions and applied to the delivery or storage of H_2, thus functioning as a charge–discharge system to obtain H_2 on demand, generating an ideal carbon-neutral cycle. Hence, it is expected that in the coming years, an increasing number of research groups will be interested in this promising topic, which will be crucial to developing an additional alternative for an energy future based on an environmentally sustainable approach.

Author Contributions: P.R.-G. wrote the manuscript, M.N.-G. designed the structure of the manuscript and reviewed the paper, and D.C.-A. reviewed the paper. All authors have read and agreed to the published version of the manuscript.

Funding: This work is part of the R + D + I project PID2021-123079OB-I00, funded by MCIN/AEI/10.13039/501100011033; "ERDF: A Way of Making Europe"; and also the project TED2021-131324B-C22, funded by MCIN/AEI/10.13039/501100011033 and by the "European Union NextGenerationEU/PRTR. M.N.G. would like to express thanks for the grant RYC2021-034199-I funded by MCIN/AEI/10.13039/501100011033 and by "ESF Investing in Your Future".

Data Availability Statement: Not applicable.

Conflicts of Interest: The authors declare no conflict of interest.

Abbreviations

AC	Activated carbon
ac STEM	Aberration-corrected scanning transmission electron microscopy
CNTs	Carbon nanotubes
DFT	Density functional theory
FA	Formic acid
LA	L-arginine
LOHCs	Liquid organic hydrogen carriers
mgp-C_3N_4	Mesoporous carbon nitride
MHCS	Mesoporous hollow carbon spheres
NEXAFS	Near-edge X-ray absorption fine structure
NMC	N-doped mesoporous carbon
NPs	Nanoparticles
SF	Sodium formate
TPAL	Terephthalaldehyde
TOF	Turnover frequency
TON	Turnover number
XPS	X-ray photoelectron spectroscopy

References

1. Armaroli, N.; Balzani, V. The future of energy supply: Challenges and opportunities. *Angew. Chem. Int. Ed.* **2007**, *46*, 52–66. [CrossRef] [PubMed]
2. Chow, J.; Kopp, R.J.; Portney, P.R. Energy Resources and Global Development. *Science* **2023**, *302*, 1528–1531. [CrossRef] [PubMed]
3. Papadis, E.; Tsatsaronis, G. Challenges in the decarbonization of the energy sector. *Energy* **2020**, *205*, 118025. [CrossRef]
4. Proost, J. Critical assessment of the production scale required for fossil parity of green electrolytic hydrogen. *Int. J. Hydrogen Energy* **2020**, *45*, 17067–17075. [CrossRef]
5. Muthukumar, P.; Kumar, A.; Afzal, M.; Bhogilla, S.; Sharma, P.; Parida, A.; Jana, S.; Kumar, E.A.; Pai, R.K.; Jain, I. Review on large-scale hydrogen storage systems for better sustainability. *Int. J. Hydrogen Energy* **2023**, *48*, 33223–33259. [CrossRef]
6. Aakko-Saksa, P.T.; Cook, C.; Kiviaho, J.; Repo, T. Liquid organic hydrogen carriers for transportation and storing of renewable energy—Review and discussion. *J. Power Source* **2018**, *396*, 803–823. [CrossRef]
7. Rao, P.C.; Yoon, M. Potential Liquid-Organic Hydrogen Carrier (LOHC) Systems: A Review on Recent Progress. *Energies* **2020**, *13*, 6040. [CrossRef]
8. Bulushev, D.A.; Ross, J.R.H. Towards Sustainable Production of Formic Acid. *ChemSusChem* **2018**, *11*, 821–836. [CrossRef]
9. Enthaler, S.; von Langermann, J.; Schmidt, T. Carbon dioxide and formic acid—The couple for environmental-friendly hydrogen storage? *Energy Environ. Sci.* **2020**, *3*, 1207–1217. [CrossRef]
10. Wu, Y.; Wen, M.; Navlani-García, M.; Kuwahara, Y.; Mori, K.; Yamashita, H. Palladium Nanoparticles Supported on Titanium-Doped Graphitic Carbon Nitride for Formic Acid Dehydrogenation. *Chem. Asian J.* **2017**, *12*, 860–867. [CrossRef]
11. Navlani-García, M.; Salinas-Torres, D.; Vázquez-Álvarez, F.D.; Cazorla-Amorós, D. Formic acid dehydrogenation attained by Pd nanoparticles-based catalysts supported on MWCNT-C3N4 composites. *Catal. Today* **2022**, *397–399*, 428–435. [CrossRef]
12. Ortega-Murcia, A.; Navlani-García, M.; Morallón, E.; Cazorla-Amorós, D. MWCNT-Supported PVP-Capped Pd Nanoparticles as Efficient Catalysts for the Dehydrogenation of Formic Acid. *Front. Chem.* **2020**, *8*, 534710. [CrossRef] [PubMed]
13. Sun, Q.; Chen, B.; Wang, N.; He, Q.; Chang, A.; Yang, C.M.; Asakura, H.; Tanaka, T.; Hülsey, M.J.; Wang, C.-H.; et al. Zeolite-Encaged Pd–Mn Nanocatalysts for CO_2 Hydrogenation and Formic Acid Dehydrogenation. *Angew. Chem. Int. Ed.* **2020**, *59*, 20183–20191. [CrossRef] [PubMed]
14. Jeon, H.-J.; Chung, Y.-M. Hydrogen production from formic acid dehydrogenation over Pd/C catalysts: Effect of metal and support properties on the catalytic performance. *Appl. Catal. B Environ.* **2017**, *210*, 212–222. [CrossRef]

15. Grasemann, M.; Laurenczy, G. Formic acid as a hydrogen source—Recent developments and future trends. *Energy Environ. Sci.* **2012**, *5*, 8171–8181. [CrossRef]
16. Yadav, M.; Xu, Q. Liquid-phase chemical hydrogen storage materials. *Energy Environ. Sci.* **2012**, *5*, 9698–9725. [CrossRef]
17. Jiang, H.; Singh, S.K.; Yan, J.; Zhang, X.; Xu, Q. Liquid-Phase Chemical Hydrogen Storage: Catalytic Hydrogen Generation under Ambient Conditions. *ChemSusChem* **2010**, *3*, 541–549. [CrossRef]
18. Bulushev, D.A.; Sobolev, V.I.; Pirutko, L.V.; Starostina, A.V.; Asanov, I.P.; Modin, E.; Chuvilin, A.L.; Gupta, N.; Okotrub, A.V.; Bulusheva, L.G. Hydrogen production from formic acid over Au catalysts supported on carbon: Comparison with Au catalysts supported on SiO_2 and Al_2O_3. *Catalysts* **2019**, *9*, 376. [CrossRef]
19. Bi, Q.-Y.; Lin, J.-D.; Liu, Y.-M.; Huang, F.-Q.; Cao, Y. Promoted hydrogen generation from formic acid with amines using Au/ZrO_2 catalyst. *Int. J. Hydrogen Energy* **2016**, *41*, 21193–21202. [CrossRef]
20. Gonçalves, L.P.; Christensen, D.B.; Meledina, M.; Salonen, L.M.; Petrovykh, D.Y.; Carbó, A.; Sousa, J.P.S.; Soares, O.S.G.P.; Pereira, M.F.R.; Kegnaes, S.E.; et al. Selective formic acid dehydrogenation at low temperature over a RuO_2/COF pre-catalyst synthesized on the gram scale. *Catal. Sci. Technol.* **2020**, *10*, 1991–1995. [CrossRef]
21. Podyacheva, O.; Lisitsyn, A.; Kibis, L.; Boronin, A.; Stonkus, O.; Zaikovskii, V.; Suboch, A.; Sobolev, V.; Parmon, V. Nitrogen doped carbon nanotubes and nanofibers for green hydrogen production: Similarities in the nature of nitrogen species, metal–nitrogen interaction, and catalytic properties. *Energies* **2019**, *12*, 3976. [CrossRef]
22. Guo, L.; Zhuge, K.; Yan, S.; Wang, S.; Zhao, J.; Wang, S.; Qiao, P.; Liu, J.; Mou, X.; Zhu, H.; et al. Defect-driven nanostructuring of low-nuclearity Pt-Mo ensembles for continuous gas-phase formic acid dehydrogenation. *Nat. Commun.* **2023**, *14*, 7518. [CrossRef] [PubMed]
23. Martin, C.; Quintanilla, A.; Vega, G.; Casas, J.A. Formic acid-to-hydrogen on Pd/AC catalysts: Kinetic study with catalytic deactivation. *Appl. Catal. B Environ.* **2022**, *317*, 121802. [CrossRef]
24. Zacharska, M.; Bulusheva, L.G.; Lisitsyn, A.S.; Beloshapkin, S.; Guo, Y.; Chuvilin, A.L.; Shlyakhova, E.V.; Podyacheva, O.Y.; Leahy, J.J.; Okotrub, A.V.; et al. Factors influencing the performance of Pd/C catalysts in the green production of hydrogen from formic acid. *ChemSusChem* **2017**, *10*, 720–730. [CrossRef] [PubMed]
25. Kosider, A.; Blaumeiser, D.; Schötz, S.; Preuster, P.; Bösmann, A.; Wasserscheid, P.; Libuda, J.; Bauer, T. Enhancing the feasibility of Pd/C-catalyzed formic acid decomposition for hydrogen generation–catalyst pretreatment, deactivation, and regeneration. *Cat. Sci. Technol.* **2021**, *11*, 4259–4271. [CrossRef]
26. Navlani-García, M.; Mori, K.; Kuwahara, Y.; Yamashita, H. Recent strategies targeting efficient hydrogen production from chemical hydrogen storage materials over carbon-supported catalysts. *NPG Asia Mater.* **2018**, *10*, 277–292. [CrossRef]
27. Lvarez, A.; Bansode, A.; Urakawa, A.; Bavykina, A.V.; Wezendonk, T.A.; Makkee, M.; Gascon, J.; Kapteijn, F. Challenges in the greener production of formates/formic acid, methanol, and DME by heterogeneously catalyzed CO_2 hydrogenation processes. *Chem. Rev.* **2017**, *117*, 9804–9838. [CrossRef]
28. Li, S.; Zhou, Y.; Kang, X.; Liu, D.; Gu, L.; Zhang, Q.; Yan, J.; Jiang, Q. A Simple and Effective Principle for a Rational Design of Heterogeneous Catalysts for Dehydrogenation of Formic Acid. *Adv. Mater.* **2019**, *31*, e1806781. [CrossRef]
29. Wakai, C.; Yoshida, K.; Tsujino, Y.; Matubayasi, N.; Nakahara, M. Effect of concentration, acid, temperature, and metal on competitive reaction pathways for decarbonylation and decarboxylation of formic acid in hot water. *Chem. Lett.* **2004**, *33*, 572–573. [CrossRef]
30. Mellmann, D.; Sponholz, P.; Junge, H.; Beller, M. Formic acid as a hydrogen storage material—Development of homogeneous catalysts for selective hydrogen release. *Chem. Soc. Rev.* **2016**, *45*, 3954–3988. [CrossRef]
31. Sordakis, K.; Tang, C.; Vogt, L.K.; Junge, H.; Dyson, P.J.; Beller, M.; Laurenczy, G. Homogeneous Catalysis for Sustainable Hydrogen Storage in Formic Acid and Alcohols. *Chem. Rev.* **2018**, *118*, 372–433. [CrossRef] [PubMed]
32. Onishi, N.; Laurenczy, G.; Beller, M.; Himeda, Y. Recent progress for reversible homogeneous catalytic hydrogen storage in formic acid and in methanol. *Coord. Chem. Rev.* **2018**, *373*, 317–332. [CrossRef]
33. Sun, Q.; Wang, N.; Xu, Q.; Yu, J. Nanopore-Supported Metal Nanocatalysts for Efficient Hydrogen Generation from Liquid-Phase Chemical Hydrogen Storage Materials. *Adv. Mater.* **2020**, *32*, e2001818. [CrossRef] [PubMed]
34. Xie, W.; Schlücker, S. Surface-enhanced Raman spectroscopic detection of molecular chemo- and plasmo-catalysis on noble metal nanoparticles. *Chem. Commun.* **2018**, *54*, 2326–2336. [CrossRef]
35. He, N.; Li, Z.H. Palladium-atom catalyzed formic acid decomposition and the switch of reaction mechanism with temperature. *Phys. Chem. Chem. Phys.* **2016**, *18*, 10005–10017. [CrossRef]
36. Navlani-García, M.; Mori, K.; Salinas-Torres, D.; Kuwahara, Y.; Yamashita, H. New approaches toward the hydrogen production from formic acid dehydrogenation over Pd-based heterogeneous catalysts. *Front. Mater.* **2019**, *6*, 439363. [CrossRef]
37. Mori, K.; Masuda, S.; Tanaka, H.; Yoshizawa, K.; Che, M.; Yamashita, H. Phenylamine-functionalized mesoporous silica supported PdAg nanoparticles: A dual heterogeneous catalyst for formic acid/CO_2-mediated chemical hydrogen delivery/storage. *Chem. Commun.* **2017**, *53*, 4677–4680. [CrossRef]
38. Jin, M.-H.; Park, J.-H.; Oh, D.; Park, J.-S.; Lee, K.-Y.; Lee, D.-W. Effect of the amine group content on catalytic activity and stability of mesoporous silica supported Pd catalysts for additive-free formic acid dehydrogenation at room temperature. *Int. J. Hydrogen Energy* **2019**, *44*, 4737–4744. [CrossRef]

39. Bulut, A.; Yurderi, M.; Karatas, Y.; Zahmakiran, M.; Kivrak, H.; Gulcan, M.; Kaya, M. Pd-MnOx nanoparticles dispersed on amine-grafted silica: Highly efficient nanocatalyst for hydrogen production from additive-free dehydrogenation of formic acid under mild conditions. *Appl. Catal. B* **2015**, *164*, 324–333. [CrossRef]
40. Wen, M.; Mori, K.; Kuwahara, Y.; Yamashita, H. Plasmonic Au@Pd nanoparticles supported on a basic metal-organic framework: Synergic boosting of H_2 production from formic acid. *ACS Energy Lett.* **2017**, *2*, 1–7. [CrossRef]
41. Zhang, A.; Xia, J.; Yao, Q.; Lu, Z.H. Pd–WOx heterostructures immobilized by MOFs-derived carbon cage for formic acid dehydrogenation. *Appl. Catal. B* **2022**, *309*, 121278. [CrossRef]
42. Martis, M.; Mori, K.; Fujiwara, K.; Ahn, W.S.; Yamashita, H. Amine-functionalized MIL-125 with embedded palladium nanoparticles as an efficient catalyst for dehydrogenation of formic acid at ambient temperature. *J. Phys. Chem. C* **2013**, *117*, 22805–22810. [CrossRef]
43. Navlani-García, M.; Martis, M.; Lozano-Castelló, D.; Cazorla-Amorós, D.; Mori, K.; Yamashita, H. Investigation of Pd nanoparticles supported on zeolites for hydrogen production from formic acid dehydrogenation. *Catal. Sci. Technol.* **2015**, *5*, 364–371. [CrossRef]
44. Navlani-García, M.; Mori, K.; Nozaki, A.; Kuwahara, Y.; Yamashita, H. Screening of Carbon-Supported PdAg Nanoparticles in the Hydrogen Production from Formic Acid. *Ind. Eng. Chem. Res.* **2016**, *55*, 7612–7620. [CrossRef]
45. Jia, L.; Bulushev, D.A.; Beloshapkin, S.; Ross, J.R. Hydrogen production from formic acid vapour over a Pd/C catalyst promoted by potassium salts: Evidence for participation of buffer-like solution in the pores of the catalyst. *Appl. Catal. B Environ.* **2014**, *160*, 35–43. [CrossRef]
46. Bulushev, D.A.; Zacharska, M.; Lisitsyn, A.S.; Podyacheva, O.Y.; Hage, F.S.; Ramasse, Q.M.; Bangert, U.; Bulusheva, L.G. Single atoms of Pt-group metals stabilized by N-doped carbon nanofibers for efficient hydrogen production from formic acid. *ACS Catal.* **2016**, *6*, 3442–3451. [CrossRef]
47. Podyacheva, O.Y.; Bulushev, D.A.; Suboch, A.N.; Svintsitskiy, D.A.; Lisitsyn, A.S.; Modin, E.; Chuvilin, A.; Gerasimov, E.Y.; Sobolev, V.I.; Parmon, V.N. Highly stable single-atom catalyst with ionic Pd active sites supported on N-doped carbon nanotubes for formic acid decomposition. *ChemSusChem* **2018**, *11*, 3724–3727. [CrossRef]
48. Bulushev, D.A.; Beloshapkin, S.; Ross, J.R. Hydrogen from formic acid decomposition over Pd and Au catalysts. *Catal. Today* **2010**, *154*, 7–12. [CrossRef]
49. Li, J.; Chen, W.; Zhao, H.; Zheng, X.; Wu, L.; Pan, H.; Zhu, J.; Chen, Y.; Lu, J. Size-dependent catalytic activity over carbon-supported palladium nanoparticles in dehydrogenation of formic acid. *J. Catal.* **2017**, *352*, 371–381. [CrossRef]
50. Mori, K.; Hara, T.; Mizugaki, T.; Ebitani, K.; Kaneda, K. Hydroxyapatite-supported palladium nanoclusters: A highly active heterogeneous catalyst for selective oxidation of alcohols by use of molecular oxygen. *J. Am. Chem. Soc.* **2004**, *126*, 10657–10666. [CrossRef]
51. Navlani-García, M.; Mori, K.; Nozaki, A.; Kuwahara, Y.; Yamashita, H. Investigation of Size Sensitivity in the Hydrogen Production from Formic Acid over Carbon-Supported Pd Nanoparticles. *ChemistrySelect* **2016**, *1*, 1879–1886. [CrossRef]
52. Navlani-García, M.; Salinas-Torres, D.; Mori, K.; Léonard, A.F.; Kuwahara, Y.; Job, N.; Yamashita, H. Insights on palladium decorated nitrogen-doped carbon xerogels for the hydrogen production from formic acid. *Catal. Today* **2019**, *324*, 90–96. [CrossRef]
53. Chaparro-Garnica, J.; Navlani-García, M.; Salinas-Torres, D.; Morallón, E.; Cazorla-Amorós, D. Highly Stable N-Doped Carbon-Supported Pd-Based Catalysts Prepared from Biomass Waste for H_2 Production from Formic Acid. *ACS Sustain. Chem. Eng.* **2020**, *8*, 15030–15043. [CrossRef]
54. Shao, X.; Miao, X.; Tian, F.; Bai, M.; Guo, X.; Wang, W.; Zhao, Z.; Ji, X.; Li, M.; Deng, F. Amine-functionalized hierarchically porous carbon supported Pd nanocatalysts for highly efficient H2 generation from formic acid with fast-diffusion channels. *J. Energy Chem.* **2023**, *76*, 249–258. [CrossRef]
55. Masuda, S.; Mori, K.; Futamura, Y.; Yamashita, H. PdAg Nanoparticles Supported on Functionalized Mesoporous Carbon: Promotional Effect of Surface Amine Groups in Reversible Hydrogen Delivery/Storage Mediated by Formic Acid/CO_2. *ACS Catal.* **2018**, *8*, 2277–2285. [CrossRef]
56. Kim, Y.; Kim, D.H. Hydrogen production from formic acid dehydrogenation over a Pd supported on N-doped mesoporous carbon catalyst: A role of nitrogen dopant. *Appl. Catal. A Gen.* **2020**, *608*, 117887. [CrossRef]
57. Salinas-Torres, D.; Navlani-García, M.; Mori, K.; Kuwahara, Y.; Yamashita, H. Nitrogen-doped carbon materials as a promising platform toward the efficient catalysis for hydrogen generation. *Appl. Catal. A Gen.* **2019**, *571*, 25–41. [CrossRef]
58. Nishchakova, A.D.; Bulushev, D.A.; Stonkus, O.A.; Asanov, I.P.; Ishchenko, A.V.; Okotrub, A.V.; Bulusheva, L.G. Effects of the Carbon Support Doping with Nitrogen for the Hydrogen Production from Formic Acid over Ni Catalysts. *Energies* **2019**, *12*, 4111. [CrossRef]
59. Yao, M.; Liang, W.; Chen, H.; Zhang, X. Efficient Hydrogen Production from Formic Acid Using Nitrogen-Doped Activated Carbon Supported Pd. *Catal. Lett.* **2020**, *150*, 2377–2384. [CrossRef]
60. Wang, H.; Gu, X.-K.; Zheng, X.; Pan, H.; Zhu, J.; Chen, S.; Cao, L.; Li, W.-X.; Lu, J. Disentangling the size-dependent geometric and electronic effects of palladium nanocatalysts beyond selectivity. *Sci. Adv.* **2019**, *5*, eaat6413. [CrossRef]
61. Jeon, M.; Han, D.J.; Lee, K.-S.; Choi, S.H.; Han, J.; Nam, S.W.; Jang, S.C.; Park, H.S.; Yoon, C.W. Electronically modified Pd catalysts supported on N-doped carbon for the dehydrogenation of formic acid. *Int. J. Hydrogen Energy* **2016**, *41*, 15453–15461. [CrossRef]
62. Chen, Y.; Li, X.; Wei, Z.; Mao, S.; Deng, J.; Cao, Y.; Wang, Y. Efficient synthesis of ultrafine Pd nanoparticles on an activated N-doping carbon for the decomposition of formic acid. *Catal. Commun.* **2018**, *108*, 55–58. [CrossRef]

63. Bulushev, D.A.; Zacharska, M.; Shlyakhova, E.V.; Chuvilin, A.L.; Guo, Y.; Beloshapkin, S.; Okotrub, A.V.; Bulesheva, L.G. Single Isolated Pd^{2+} Cations Supported on N-Doped Carbon as Active Sites for Hydrogen Production from Formic Acid Decomposition. *ACS Catal.* **2016**, *6*, 681–691. [CrossRef]
64. Bulushev, D.A.; Golub, F.S.; Trubina, S.V.; Zvereva, V.V.; Gerasimov, E.Y.; Prosvirin, I.P.; Navlani-García, M.; Jena, H.S. Pd Active Sites on Covalent Triazine Frameworks for Catalytic Hydrogen Production from Formic Acid. *ACS Appl. Nano Mater.* **2023**, *6*, 13551–13560. [CrossRef]
65. Liu, D.; Gao, Z.; Wang, X.; Zeng, J.; Li, Y. DFT study of hydrogen production from formic acid decomposition on Pd-Au alloy nanoclusters. *Appl. Surf. Sci.* **2017**, *426*, 194–205. [CrossRef]
66. Shu, J.; Grandjean, B.P.A.; Van Neste, A.; Kaliaguine1, S. Catalytic palladium-based membrane reactors: A review. *Can. J. Chem. Eng.* **1991**, *69*, 1036–1060. [CrossRef]
67. Navlani-García, M.; Salinas-Torres, D.; Cazorla-Amorós, D. Hydrogen Production from Formic Acid Attained by Bimetallic Heterogeneous PdAg Catalytic Systems. *Energies* **2019**, *12*, 4027. [CrossRef]
68. Kim, Y.; Kim, D.H. Elucidating the alloying effect of PdAg/CNT catalysts on formic acid dehydrogenation with kinetic isotope effect. *Mol. Catal.* **2023**, *547*, 113343. [CrossRef]
69. Nabid, M.R.; Bide, Y.; Etemadi, B. Ag@Pd nanoparticles immobilized on a nitrogen-doped graphene carbon nanotube aerogel as a superb catalyst for the dehydrogenation of formic acid. *N. J. Chem.* **2017**, *41*, 10773–10779. [CrossRef]
70. Chaparro-Garnica, J.; Navlani-García, M.; Salinas-Torres, D.; Berenguer-Murcia, Á.; Morallón, E.; Cazorla-Amorós, D. Efficient production of hydrogen from a valuable CO_2-derived molecule: Formic acid dehydrogenation boosted by biomass waste-derived catalysts. *Fuel* **2022**, *320*, 123900. [CrossRef]
71. Jiang, Y.; Fan, X.; Chen, M.; Xiao, X.; Zhang, Y.; Wang, C.; Chen, L. AuPd Nanoparticles Anchored on Nitrogen-Decorated Carbon Nanosheets with Highly Efficient and Selective Catalysis for the Dehydrogenation of Formic Acid. *J. Phys. Chem. C* **2018**, *122*, 4792–4801. [CrossRef]
72. Hong, W.; Kitta, M.; Tsumori, N.; Himeda, Y.; Autrey, T.; Xu, Q. Immobilization of highly active bimetallic PdAu nanoparticles onto nanocarbons for dehydrogenation of formic acid. *J. Mater. Chem. A Mater.* **2019**, *7*, 18835–18839. [CrossRef]
73. Navlani-García, M.; Salinas-Torres, D.; Mori, K.; Kuwahara, Y.; Yamashita, H. Enhanced formic acid dehydrogenation by the synergistic alloying effect of PdCo catalysts supported on graphitic carbon nitride. *Int. J. Hydrogen Energy* **2019**, *44*, 28483–28493. [CrossRef]
74. Tamarany, R.; Shin, D.Y.; Kang, S.; Jeong, H.; Kim, J.; Kim, J.; Yoon, C.W.; Lim, D.-H. Formic acid dehydrogenation over PdNi alloys supported on N-doped carbon: Synergistic effect of Pd–Ni alloying on hydrogen release. *Phys. Chem. Chem. Phys.* **2021**, *23*, 11515–11527. [CrossRef] [PubMed]
75. Mori, K.; Tanaka, H.; Dojo, M.; Yoshizawa, K.; Yamashita, H. Synergic Catalysis of PdCu Alloy Nanoparticles within a Macroreticular Basic Resin for Hydrogen Production from Formic Acid. *Chem. A Eur. J.* **2015**, *21*, 12085–12092. [CrossRef] [PubMed]
76. Yurderi, M.; Bulut, A.; Zahmakiran, M.; Kaya, M. Carbon supported trimetallic PdNiAg nanoparticles as highly active, selective and reusable catalyst in the formic acid decomposition. *Appl. Catal. B Environ.* **2014**, *160–161*, 514–524. [CrossRef]
77. Wang, Z.-L.; Ping, Y.; Yan, J.-M.; Wang, H.-L.; Jiang, Q. Hydrogen generation from formic acid decomposition at room temperature using a NiAuPd alloy nanocatalyst. *Int. J. Hydrogen Energy* **2014**, *39*, 4850–4856. [CrossRef]
78. Dong, Z.; Li, F.; He, Q.; Xiao, X.; Chen, M.; Wang, C.; Fan, X.; Chen, L. PdCoNi nanoparticles supported on nitrogen-doped porous carbon nanosheets for room temperature dehydrogenation of formic acid. *Int. J. Hydrogen Energy* **2019**, *44*, 11675–11683. [CrossRef]
79. Liu, D.-X.; Zhou, Y.-T.; Zhu, Y.-F.; Chen, Z.-Y.; Yan, J.-M.; Jiang, Q. Tri-metallic AuPdIr nanoalloy towards efficient hydrogen generation from formic acid. *Appl. Catal. B Environ.* **2022**, *309*, 121228. [CrossRef]
80. Mori, K.; Dojo, M.; Yamashita, H. Pd and Pd–Ag nanoparticles within a macroreticular basic resin: An efficient catalyst for hydrogen production from formic acid decomposition. *ACS Catal.* **2013**, *3*, 1114–1119. [CrossRef]
81. Lv, Q.; Meng, Q.; Liu, W.; Sun, N.; Jiang, K.; Ma, L.; Peng, Z.; Cai, W.-B.; Liu, C.; Ge, J.; et al. Pd–PdO interface as active site for HCOOH selective dehydrogenation at ambient condition. *J. Phys. Chem. C* **2018**, *122*, 2081–2088. [CrossRef]
82. Lee, J.H.; Ryu, J.; Kim, J.Y.; Nam, S.-W.; Han, J.H.; Lim, T.-H.; Gautam, S.; Chae, K.H.; Yoon, C.W. Carbon dioxide mediated, reversible chemical hydrogen storage using a Pd nanocatalyst supported on mesoporous graphitic carbon nitride. *J. Mater. Chem. A Mater.* **2014**, *2*, 9490–9495. [CrossRef]
83. Bi, Q.; Lin, J.; Liu, Y.; Du, X.; Wang, J.; He, H.; Cao, Y. An Aqueous Rechargeable Formate-Based Hydrogen Battery Driven by Heterogeneous Pd Catalysis. *Angew. Chem. Int. Ed.* **2014**, *53*, 13583–13587. [CrossRef] [PubMed]
84. Koh, K.; Jeon, M.; Chevrier, D.M.; Zhang, P.; Yoon, C.W.; Asefa, T. Novel nanoporous N-doped carbon-supported ultrasmall Pd nanoparticles: Efficient catalysts for hydrogen storage and release. *Appl. Catal. B Environ.* **2017**, *203*, 820–828. [CrossRef]
85. Yan, N.; Philippot, K. Transformation of CO_2 by using nanoscale metal catalysts: Cases studies on the formation of formic acid and dimethylether. *Curr. Opin. Chem. Eng.* **2018**, *20*, 86–92. [CrossRef]
86. Verma, P.; Zhang, S.; Song, S.; Mori, K.; Kuwahara, Y.; Wen, M.; Yamashita, H.; An, T. Recent strategies for enhancing the catalytic activity of CO_2 hydrogenation to formate/formic acid over Pd-based catalyst. *J. CO_2 Util.* **2021**, *54*, 101765. [CrossRef]
87. Kumaravel, V.; Bartlett, J.; Pillai, S.C. Photoelectrochemical Conversion of Carbon Dioxide (CO_2) into Fuels and Value-Added Products. *ACS Energy Lett.* **2020**, *5*, 486–519. [CrossRef]

88. Sun, Z.; Ma, T.; Tao, H.; Fan, Q.; Han, B. Fundamentals and Challenges of Electrochemical CO_2 Reduction Using Two-Dimensional Materials. *Chem* **2017**, *3*, 560–587. [CrossRef]
89. Sun, R.; Liao, Y.; Bai, S.-T.; Zhen, M.; Zhou, C.; Zhang, T.; Sels, B.F. Heterogeneous catalysts for hydrogenation of CO_2 and bicarbonates to formic acid and formates. *Catal. Rev.* **2018**, *60*, 566–593.
90. Jessop, P.G.; Ikariya, T.; Noyori, R. Homogeneous Hydrogenation of Carbon Dioxide. *Chem. Rev.* **1995**, *95*, 259–272. [CrossRef]
91. Sun, R.; Liao, Y.; Bai, S.-T.; Zheng, M.; Zhou, C.; Zhang, T.; Sels, B.F. Heterogeneous catalysts for CO_2 hydrogenation to formic acid/formate: From nanoscale to single atom. *Energy Environ. Sci.* **2021**, *14*, 1247–1285. [CrossRef]
92. Jessop, P.G.; Joó, F.; Tai, C.-C. Recent advances in the homogeneous hydrogenation of carbon dioxide. *Coord. Chem. Rev.* **2004**, *248*, 2425–2442. [CrossRef]
93. Shao, X.; Xu, J.; Huang, Y.; Su, X.; Duan, H.; Wang, X.; Zhang, T. Pd@C_3N_4 nanocatalyst for highly efficient hydrogen storage system based on potassium bicarbonate/formate. *AIChE J.* **2016**, *62*, 2410–2418. [CrossRef]
94. Wang, F.; Xu, J.; Shao, X.; Su, X.; Huang, Y.; Zhang, T. Palladium on Nitrogen-Doped Mesoporous Carbon: A Bifunctional Catalyst for Formate-Based, Carbon-Neutral Hydrogen Storage. *ChemSusChem* **2016**, *9*, 246–251. [CrossRef] [PubMed]
95. Song, H.; Zhang, N.; Zhong, C.; Liu, Z.; Xiao, M.; Gai, H. Hydrogenation of CO_2 into formic acid using a palladium catalyst on chitin. *New J. Chem.* **2017**, *41*, 9170–9177. [CrossRef]
96. Yang, G.; Kuwahara, Y.; Mori, K.; Louis, C.; Yamashita, H. PdAg alloy nanoparticles encapsulated in N-doped microporous hollow carbon spheres for hydrogenation of CO_2 to formate. *Appl. Catal. B Environ.* **2021**, *283*, 119628. [CrossRef]
97. Yang, G.; Kuwahara, Y.; Mori, K.; Louis, C.; Yamashita, H. Pd-Cu alloy nanoparticles confined within mesoporous hollow carbon spheres for the hydrogenation of CO_2 to formate. *J. Phys. Chem. C* **2021**, *125*, 3961–3971. [CrossRef]
98. Nguyen, L.T.M.; Park, H.; Banu, M.; Kim, J.Y.; Youn, D.H.; Magesh, G.; Kim, W.Y.; Lee, J.S. Catalytic CO_2 hydrogenation to formic acid over carbon nanotube-graphene supported PdNi alloy catalysts. *RSC Adv.* **2015**, *5*, 105560–105566. [CrossRef]
99. Zell, T.; Langer, R. CO_2-based hydrogen storage—Formic acid dehydrogenation. *Phys. Sci. Rev.* **2018**, *3*, 20170012. [CrossRef]
100. Chatterjee, S.; Dutta, I.; Lum, Y.; Lai, Z.; Huang, K.-W. Enabling storage and utilization of low-carbon electricity: Power to formic acid. *Energy Environ. Sci.* **2021**, *14*, 1194–1246. [CrossRef]
101. Su, J.; Yang, L.; Lu, M.; Lin, H. Highly Efficient Hydrogen Storage System Based on Ammonium Bicarbonate/Formate Redox Equilibrium over Palladium Nanocatalysts. *ChemSusChem* **2015**, *8*, 813–816. [CrossRef] [PubMed]
102. Zhou, Y.; Huang, Y.; Jin, B.; Luo, X.; Liang, Z. Pd Nanoclusters-Based Catalysts with Schiff Base Modifying Carrier for CO_2 Hydrogenation to Formic Acid. *Ind. Eng. Chem. Res.* **2019**, *58*, 44–52. [CrossRef]
103. Soma-Noto, Y.; Sachtler, W.M.H. Infrared spectra of carbon monoxide adsorbed on supported palladium and palladium-silver alloys. *J. Catal.* **1974**, *32*, 315–324. [CrossRef]
104. Tedsree, K.; Li, T.; Jones, S.; Chan, C.W.A.; Yu, K.M.K.; Bagot, P.A.J.; Marquis, E.A.; Smith, G.D.W.; Tsang, S.C.E. Hydrogen production from formic acid decomposition at room temperature using a Ag–Pd core–shell nanocatalyst. *Nat. Nanotechnol.* **2011**, *6*, 302–307. [CrossRef]
105. Wang, H.-X.; Toh, W.L.; Tang, B.Y.; Surendranath, Y. Metal surfaces catalyse polarization-dependent hydride transfer from H_2. *Nat. Catal.* **2023**, *6*, 351–362. [CrossRef]